The Global Precipitation Measurement (GPM) mission's scientific achievements and societal contributions: reviewing four years of advanced rain and snow observations

Revisions submitted to: Quarterly Journal of the Royal Meteorological Society. Special issue: *Advances in remote sensing of rainfall and snowfall*

Authors:

Gail Skofronick-Jackson[1], Dalia Kirschbaum[1], Walter Petersen[2], George Huffman[1], Chris Kidd[3,1], Erich Stocker[1], Ramesh Kakar[4]

1. Code 612.0, NASA Goddard Space Flight Center, Greenbelt, MD
2. ST11, NASA Marshall Space Flight Center, Earth Sciences Office, National Space and Technology Center, Huntsville, AL
3. Earth System Science Interdisciplinary Center, University of Maryland, College Park, MD
4. NASA Headquarters, Washington, D.C.

Abstract

Precipitation represents a life-critical energy and hydrologic exchange between the Earth's atmosphere and its surface. As such, knowledge of where, when, and how much rain and snow falls is essential for scientific research and societal applications. Building on the 17-year success of the Tropical Rainfall Measurement Mission (TRMM), the Global Precipitation Measurement (GPM) Core Observatory (GPM-CO) is the first U.S. National Aeronautical and Space Administration (NASA) satellite mission specifically designed with sensors to observe the structure and intensities of both rain and falling snow. The GPM-CO has proved to be a worthy successor to TRMM, extending and improving high-quality active and passive microwave observations across all times of day. The GPM-CO launched in early 2014, is a joint mission between NASA and the Japanese Aerospace Exploration Agency (JAXA), with sensors that include the NASA-provided GPM Microwave Imager and the JAXA-provided Dual-frequency Precipitation Radar. These sensors were devised with high accuracy standards enabling them to be used as a reference for inter-calibrating a constellation of partner satellite data. These inter-

calibrated partner satellite retrievals are used with infrared data to produce merged precipitation estimates at temporal scales of 30 minutes and spatial scales of 0.1° x 0.1°. Precipitation estimates from the GPM-CO and partner constellation satellites, provided in near real time and later reprocessed with all ancillary data, are an indispensable source of precipitation data for operational and scientific users. Advances have been made using GPM data, primarily in improving sensor calibration, retrieval algorithms, and ground validation measurements, and used to further our understanding of the characteristics of liquid and frozen precipitation and the science of water and hydrological cycles for climate/weather forecasting. These advances have extended to societal benefits related to water resources, operational numerical weather prediction, hurricane monitoring, prediction, and disaster response, extremes, and disease.

Keywords: precipitation, satellite, rain, snow, remote sensing, applications

1. Introduction

The 21st century poses substantial challenges for the sustainable management of the Earth's water resources at all levels from the local to the global scale. The international climate community through the World Climate Research Programme (WCRP) identified seven grand challenges facing both our understanding of, and our ability to adapt to climate change (http://wcrp-climate.org/grand-challenges). Four of these challenges relate to atmospheric water: Clouds, Circulation, and Climate Sensitivity; Weather and Climate Extremes; Water for the Food Baskets of the World; and Near-Term Climate Prediction. Three basic questions posed under these challenges are: How will the availability of fresh water change in the coming decades, what is the predictability of changes in the frequency and intensity of extremes at seasonal to decadal

time scales, and how does convection shape cloud feedbacks? Central to these questions is the need for better measurements of precipitation, from observing global patterns, to local scales where it has the most profound societal impact, and to microphysical scales to study the characteristics of rain and snow hydrometeors.

The Global Precipitation Measurement (GPM) mission is a scientific undertaking to understand the physics and space-time variability of the Earth's global precipitation as a key component of its weather, climate, and hydrological systems. In 2014, NASA and the Japan Aerospace Exploration Agency (JAXA) launched the GPM Core Observatory (GPM-CO) spacecraft. The GPM-CO carries the most advanced precipitation sensors currently in space. These sensors include the Ku and Ka-band Dual-frequency Precipitation Radar (DPR) provided by JAXA that measures three-dimensional (3D) structures of precipitation, and the GPM Microwave Imager (GMI), a well-calibrated multi-frequency radiometer capable of providing wide-swath precipitation data. The capability and swath characteristics of the GPM-CO are illustrated in Figure 1. This figure depicts the retrievals from the DPR and GMI for an overpass of a storm on 17 December 2016 with falling snow (in blues) detected and estimated over land and a thin convective line of rain (in green and red) just off the coast of North and South Carolina. The GPM-CO was designed to measure rain rates from 0.2-110.0 mm h^{-1}, to detect moderate to intense snow events, and to serve as a precipitation physics laboratory. The GPM-CO, a key part of the GPM mission (Skofronick-Jackson *et al.*, 2017), is designed to be the calibration reference standard for unifying the data from a constellation of approximately 10 partner satellites as listed in Hou *et al.* (2014). Table I provides information on the constellation members, sensors, types and launches. This constellation provides the observations for the GPM mission's next-generation, merged global precipitation estimates at high temporal and spatial

74 resolutions. The products from the Integrated Multi-satellitE Retrievals for GPM (IMERG),
75 NASA's uniformly gridded precipitation product, are one of GPM's most popular data products.
76 The four years of GPM-CO data to date, along with the 17 years of data from GPM's
77 predecessor, the Tropical Rainfall Measuring Mission (TRMM; Kummerow *et al.*, 2000), have
78 generated, and will continue to contribute to, accurate records of global, regional, convective,
79 and microphysical precipitation patterns. The inter-calibration of the TRMM Microwave Imager
80 (TMI) and pre-GPM microwave constellation sensor data to GMI's highly accurate data is
81 expected to be released in 2018, along with inter-calibrated TRMM Precipitation Radar (PR) and
82 DPR data. As a result, GPM will generate a consistent, uniform, and long-term precipitation
83 record[1] that covers both the TRMM and GPM eras, potentially stretching over 30 years subject to
84 the GPM-CO fuel, instruments, and operations.
85 The observations from GPM and TRMM can be used for characterizing changes in the
86 Earth's water cycle, quantifying freshwater fluxes and reservoirs, and advancing our predictive
87 capability of natural hazards and extreme weather events. There are far-reaching impacts for the
88 Earth system (Trenberth, 2011; Intergovernmental Panel on Climate Change (IPCC), 2014) from
89 precipitation falling on and interacting with the land surface (landslides, floods, erosion, etc.), the
90 ocean surface (salinity, sea surface temperature, density, etc.), and sea ice/glaciers (growth or
91 decay depending on rain or snow amounts). TRMM-based research has already investigated
92 changes in the global Earth system in terms of precipitation (e.g., climatology: Wang *et al.*,
93 2014; distribution: Liu and Zipser, 2009; El Nino Southern Oscillation (ENSO): Arndt *et al.*,
94 2010; Madden-Julian Oscillation (MJO): Lau and Wu, 2010). The higher frequency channels on

[1] Such long records take two forms, the Climate Data Record (CDR), which emphasizes climate-scale homogeneity, and the High Resolution Precipitation Product (HRPP), which provides the "best" snapshot estimates (Tapiador *et al.*, 2017). The individual TRMM and GPM precipitation records approximate CDRs, while IMERG is best characterized as a HRPP.

DPR (Ka) and GMI (166 and 183 GHz) were specifically added to the GPM-CO's design to be sensitive to frozen hydrometeors both above the melting layer, where frozen precipitation is responsible for 50% of global rainfall (Field and Heymsfield, 2015), and snow falling at the Earth's surface.

Precipitation information must be used synergistically with complementary observations to gain physical insights into the complex interactions between water and other components of the Earth system (e.g., Kucera *et al.*, 2013; Liu and Xie, 2017). Research has demonstrated the value of precipitation data for improving the outputs of weather prediction models (e.g., Geer *et al.*, 2017; Kim *et al.*, 2017; Chambon *et al.*, 2014). Precipitation data are critical to the assessment of global climate models and reanalysis systems, for example, Kidd *et al.* (2013) evaluated the ability of operational numerical models and satellite estimates to properly represent the diurnal cycle of precipitation, while Kim and Alexander (2013) compared TRMM estimates to five reanalysis models to investigate the variability in convectively coupled equatorial waves at submonthly time scales.

The GPM ground validation (GV) program, through its connection to atmospheric and surface modelling and observations, plays a key role in combining observations from diverse sources into a coherent framework. Direct statistical, physical, and hydrologic validation have been fundamental in verifying and improving GPM algorithms for the DPR, GMI, and combined GMI+DPR products. Field campaigns conducted by the GPM mission and its partners have explored a wide range of precipitation processes across numerous environmental settings. In the past seven years, GPM-sponsored field campaigns (see Figure 2) have observed high latitude light rain and snow in Finland (LPVEX), mid-latitude convective rain over the United States (MC3E), falling snow and cold season processes in Canada (GCPEX), heavy rainfall and

118 flooding in Iowa (IFloodS), mid-latitude continental orographic processes and
119 hydrometeorological impacts/modelling (IPHEX), and mid-latitude coastal/continental mixed-
120 phase, land/ocean and complex terrain processes (OLYMPEX).

121 From the start, GPM has been designed to be a mission with both scientific and societal
122 goals. The GPM suite of products contributes to a wide range of societal applications, many
123 initially developed with TRMM data, such as: tropical and extratropical cyclone tracking and
124 rainfall monitoring, famine early warning, drought monitoring, water resource management,
125 agricultural forecasting, numerical weather prediction, land surface modelling, global climate
126 modelling, disease monitoring, economic studies, and animal migration. Many of these
127 applications require near-real-time (NRT) data as well as longer-term, well-calibrated merged-
128 satellite precipitation information (e.g., Reed *et al.*, 2015); the GPM mission provides both of
129 these product latencies. The U.S. GPM team's IMERG product (Huffman *et al.* 2017) is being
130 used as an input for hazard assessment and forecasting for floods, landslides, fires, agriculture
131 yield prediction, famine onset, and disease outbreaks (e.g., Wu *et al*., 2014; Kirshbaum *et al*.,
132 2015a,b; Field *et al*., 2015), particularly in regions where adequate ground-based information is
133 lacking. Selected applications are also reported in Kirschbaum *et al.* (2017), and Kucera *et al.*
134 (2013). GPM data are also valuable for communities assessing the environmental impacts of
135 climate change (National Research Council, 2013), and disasters. Figure 3 shows a one-week
136 accumulation of precipitation from 16-22 July 2017, from the IMERG product. The image shows
137 important precipitation features such as the Intertropical Convergence Zone (ITCZ) located
138 along 10°N latitude across the eastern Pacific and Atlantic, and the Asian summer monsoon over
139 the Indian sub-continent and southeast Asia, along with long streaks of precipitation associated
140 with Hurricane Fernanda in the eastern Pacific between 10°-20°N and 140°-110°W.

141 Since launch, the GPM-CO instruments, spacecraft, ground systems, and data processing
142 systems have all been operating at peak performance. Notable achievements in the first three
143 years of operations include updated algorithms incorporating the improved calibration of the
144 DPR, use of the dual-frequency DPR data to construct global databases of the drop size
145 distribution (DSD) for use in single frequency radar rain retrievals, an observational database for
146 the GMI retrieval algorithm, and improved representation of light rain, falling snow, and non-
147 spherical particles. Scientifically, the GPM mission has been able to: provide a better
148 understanding of falling snow microphysics with results showing that consideration of non-
149 spherical particles in retrieval databases are essential (Olson *et al.,* 2016); use the GPM-CO data
150 as a reliable transfer standard for the constellation partner precipitation sensors to ensure
151 calibrated estimates of rain and falling snow; classify the locations of the largest, deepest, and
152 strongest precipitation systems on Earth; and provide additional benefits to weather forecasts,
153 among many applications. This paper highlights some of the technical and scientific
154 achievements of the GPM mission to date and describes how these data have contributed to
155 advancing societal applications. In Section 2 we describe GPM data products. Section 3 provides
156 an overview of GPM scientific achievements with respect to the core mission science objectives,
157 while Section 4 describes the ground validation activities. In Section 5 we describe how these
158 data products are being used by the community to enhance a range of societal applications.
159 Finally, conclusions are provided in section 6, together with future perspectives of the GPM
160 mission.
161

162 ## 2. Summary of GPM data products

163 The GPM mission has both NRT and research-quality production requirements for the
164 products listed in Table II. The NRT data are produced using GPM data enhanced with model
165 data or other forms of ancillary data. NRT products include the GMI brightness temperatures
166 (Tb; Draper *et al.*, 2015a) and precipitation retrievals from the GMI and GPM constellation
167 (using the Goddard Profiling Algorithm, GPROF; Kummerow *et al*., 2015), DPR (Masaki *et al.*,
168 2015; Seto and Iguchi, 2015), and GPM Combined Radar–Radiometer Algorithm (CORRA;
169 Grecu *et al.*, 2016). The GPM mission requires GMI products to be available within one hour of
170 data collection while both the DPR and CORRA are to be available within 3 hours of data
171 collection, 90% of the time; however, in practice the data are available on average much sooner
172 (Table III). An important NRT national product developed by the NASA team is IMERG, a
173 gridded product that uses both GPM-CO and partner satellite precipitation estimates along with
174 geostationary infrared precipitation estimates to fill in gaps between the microwave satellite
175 overpasses by Lagrangian time interpolation, or "morphing", and monthly gauge information
176 (Huffman *et al.*, 2017). As summarized in Section 3.1, the CORRA product calibrates the partner
177 satellite estimates, while the IR estimates are calibrated by the passive microwave estimates. The
178 IMERG product is available every 30 minutes at a spatial resolution of 0.1°x0.1° (or about 10
179 km x 10 km at the Equator). JAXA produces an analogous national product called Global
180 Satellite Mapping of Precipitation (GSMaP; Aonashi *et al.*, 2009) that depends on the inter-
181 calibrated brightness temperature products from the GPM constellation computed by the
182 Precipitation Processing System (PPS). All of the NRT products are also processed as research
183 products with delays of hours to months after the observation, when all the required high-quality
184 ancillary and geolocation data are received. The goal of the research products is accuracy,
185 completeness, consistency, and stability for long-term precipitation investigations.

186 In the case of IMERG, the computation is done three times to serve different communities. The
187 Early Run is computed without backward morphing and just using climatological gauge
188 information so that it can be computed within about 4 hours as input to fast-response situations,
189 such as flooding. The Late Run has backward morphing, but still only climatological gauge
190 information, allowing it to be computed about 12 hours after observations as input to next-day
191 kinds of applications, such as crop forecasting and drought analysis. The Final Run includes
192 monthly gauge analyses (from Global Precipitation Climatology Centre) and uses satellite
193 retrievals that make use of high-quality reanalyses. Its latency is about 3 months and is
194 considered the product of choice for research.

195 GPM data meet mission success requirement metrics (Skofronick-Jackson, 2017). Focusing
196 first on rainfall, Figure 4 demonstrates that the DPR, and CORRA quantify rain rates between
197 0.2 and 110 mm h^{-1}, while GMI estimates rain rates up to 60 mm h^{-1} due to the averaging of
198 strong convective cells by the coarser resolution radiometer observations. Note that at the DPR
199 (GMI) 5-km (15-km) footprint scales, rain rates $\geq$ 110 mm h^{-1} (60 mm h^{-1}) are very infrequent,
200 and make up less than 0.1% of the rain occurrences over the 2.5-year sample shown. Fig. 4
201 (right) demonstrates that GPM-CO's instantaneous rain rate bias and uncertainty are excellent,
202 being less than 50% at 1 mm h^{-1} and less than 25 % at 10 mm h^{-1}. The errors are less at 10 mm h^{-1}
203 since this is where both the Ku and Ka channels on DPR are sensitive to the rain and provide
204 additional constraints for both the DPR and CORRA algorithms. In Fig. 4e, the GMI biases run a
205 little high at 1 mm h^{-1}, probably due to the GMI mistaking some land surface features for low
206 rain rates.

207 While GPM-CO is specifically designed to also observe falling snow, the requirements were
208 only to detect falling snow. Since GPM-CO is exceeding the detection requirements by providing

209 estimates of falling snow in the DPR, CORRA, and GMI products (See Fig. 1), it is essential to
210 begin validating estimates of falling snow. Satellite algorithms for estimating falling snow have
211 yet to reach the level of maturity of the rainfall algorithms, and errors of 100-200% are not
212 unexpected. While surface observations are the natural starting point for validating satellite-
213 based estimates of falling snow, these are fraught with uncertainties (e.g., Rasmussen *et al.,*
214 2012) and are plagued with the lack of station data (Kidd *et al.*, 2017a). The National Oceanic
215 and Atmospheric Administration (NOAA) Multi-Radar Multi-Sensor (MRMS) data product (see
216 Section 4) based on surface radars provides good estimates of liquid precipitation but the
217 "quality" flag for data usage drops considerably when the precipitation is frozen or mixed-phase,
218 not least because the reflectivity-snow rate (Z-S) relationship is much more variable than the
219 reflectivity-rain rate relationship.

220 CloudSat (Stephens *et al.*, 2002) is also capable of detecting and estimating falling snow. The
221 CloudSat Cloud Profiling Radar (CPR) has a minimum detectable reflectivity of approximately -
222 29 dBZ, with falling snow (as opposed to non-precipitating ice particles) detectable to around -
223 15 dBZ. In comparison, the GPM DPR has a minimum detectable reflectivity of around 12-13
224 dBZ. In order to start assessing the impacts of minimum detectable reflectivity differences
225 between CloudSat and DPR, Figure 5 presents global difference maps (CloudSat – DPR) for
226 various cutoff thresholds of CloudSat radar reflectivity. Figure 5a demonstrates that CloudSat at
227 a -15 dBZ cutoff observes light snowfall that accumulates in the Antarctic and near Greenland
228 and, at a cutoff of 5dBZ (Fig. 5b), CloudSat is still accumulating more snow than the DPR.
229 CloudSat and DPR estimates become similar with CloudSat threshold cutoffs of between 8 and
230 12 dBZ. The sensitivity differences between CloudSat, which operates at W-band, and DPR,
231 which operates at Ku- and Ka-bands, and the different Z-S relationships used in the two

algorithms lead us to anticipate that a zero difference map might not be achievable. Figure 5 indicates that validating snow estimates will not be easy or straightforward from surface-based or satellite based estimates. Nevertheless, such comparison efforts are ongoing as shown in Tang *et al.* (2017), von Lerber *et al*. (2017). Indeed, despite the relatively high sensitivity of the DPR with a minimum detectable rate of 0.2 mmh^{-1}, the DPR has been shown to miss more than 50% of the global snowfall mass estimated by CloudSat (Casella et al., 2017). Concurrent work to improve falling snow retrieval algorithms is underway.

An additional key component in GPM is the PPS system, which captures mission operation downlinked data and archives the GPM-CO and partner brightness temperature files, the NOAA/Climate Prediction Center geo-infrared brightness temperature analyses, and ancillary data. Once PPS has acquired the requisite data, it is responsible for computing precipitation estimate products (Table II) from this data, feeding these retrievals into IMERG, hosting the resulting output files, and providing a range of user support, including value-added products. All GPM data are freely available at PPS (https://pmm.nasa.gov/data-access/downloads/gpm) while JAXA's GPM products can be obtained from https://www.gportal.jaxa.jp/gp/top.html or http://sharaku.eorc.jaxa.jp/.

3. Observational goals for GPM precipitation: microphysical to global scales

The five science goals of GPM's data products include: (1) advancing precipitation observations from space; (2) improving knowledge of precipitation systems, water cycle variability, and freshwater availability; and improving (3) hydrological, (4) climate, and (5) weather modelling and prediction. By making precipitation data available in NRT to operational agencies and users beyond the traditional science community, GPM facilitates the use of space-

255 based precipitation observations in a wide range of practical applications to directly benefit
256 society. With these goals in mind, GPM science encompasses not only scientific discovery but
257 also application-oriented research and development.
258
259 **3.1 Progress toward Advancing Precipitation Measurements**
260 The GPM-CO was specifically designed with highly calibrated instruments and enhanced
261 measurement capabilities for advancing precipitation measurements from space. These GPM-CO
262 observations aim to improve our knowledge of the microphysical properties and vertical
263 structure information of precipitating systems, while the combination of active and passive
264 observations provides a calibration standard for unifying and improving the global precipitation
265 measurements from a constellation of sensors. Assessments of GPM-CO products show that it
266 has accurate rainfall retrievals (Petersen *et al.*, 2016) with sensitivity down to 0.2 mm h^{-1} (e.g.,
267 Fig. 5 and Hamada and Takayabu, 2016), has been able to detect falling snow (e.g., You *et al.*,
268 2016; Munchak and Skofronick-Jackson, 2012; Skofronick-Jackson *et al.*, 2013), and reduced
269 the errors associated with the median mass diameter (Dm; Petersen *et al.*, 2016). Indeed, the
270 GPM DPR Version 05 single frequency Ku-band rain retrieval algorithm (DPR Algorithm
271 Theoretical Basis Document; https://pmm.nasa.gov/resources/documents/GPM) now uses a
272 global DSD database developed from three-plus years of DPR dual-frequency data. Hamada and
273 Takayabu (2016) indicate that the DPR increases observed precipitation occurrence and volume
274 by 20% and 2%, respectively, between 40˚S and 40˚N with respect to TRMM observations.
275 Battaglia *et al.* (2015) have shown that multiple scattering affects the Ka and Ku radar
276 measurements for deep convective systems and recommended a multiple-scattering forward-
277 operator-based retrieval algorithm, which has since been implemented in the Version 05 CORRA

algorithm. A better understanding of the microphysics of falling snow and frozen precipitation above the freezing layer is evolving and the results show that non-spherical particles are essential for radiative transfer modelling simulations in order to match DPR and GMI (across all frequencies) and aircraft data taken during field campaigns (e.g., Kuo *et al.*, 2016; Olson *et al.*, 2016; Molthan and Petersen, 2011).

A calibration transfer standard is facilitated by the highly stable instruments and careful attention to instrument design for the GPM-CO. With regards to the DPR, a diagnosed sidelobe clutter issue was corrected (Kubota *et al.*, 2016), and overall performance demonstrated in Kubota *et al.* (2014), Toyoshima *et al.* (2015) and Iguchi *et al.* (2016). GMI on orbit performance and calibration stability is reported in Draper et *al.* (2015a,b). Subsequently, Wentz and Draper (2016) concluded that GMI is the most accurate precipitation radiometer currently in space. To provide unified global precipitation estimates a reliable transfer standard of brightness temperatures (Tbs) between the GPM-CO and the constellation partner precipitation sensors through the inter-calibration of all the radiometer sensors has been established (Berg *et al.*, 2016). This inter-calibration effort ensures that the observed Tbs are consistent among the sensors allowing for expected differences due to variations in the observing frequencies, bandwidths, polarizations, and view angles (e.g., Wilheit *et al.*, 2015). After inter-calibration, residual differences between the GMI Tbs and those of the constellation radiometers are generally smaller than 1 K (Berg *et al.*, 2016). These GPM inter-calibrated Tbs are made available on the NASA PPS and are the first step toward unified precipitation products.

The second step of the transfer standard uses the combined DPR and GMI CORRA estimates of the GPM-CO to provide a common *a priori* precipitation/radiance database for passive microwave sensor Bayesian retrievals and is key to combining the GPM constellation

radiometers into one consistent framework to produce unified global precipitation products (Kummerow *et al.*, 2011). The current GPM-CO combined CORRA radar-radiometer algorithm architecture draws upon a rich heritage of algorithms that were developed for the TRMM mission, as well as other algorithms developed and applied to airborne radar-radiometer data. One of many challenges for the GPM GMI+DPR combined (CORRA) algorithm development is the creation of updated physical parameterizations that enable the algorithm to take better advantage of the Ka radar on the DPR and the higher frequency channels of the GMI (>89 GHz) in order to obtain greater accuracy in the measurement of light rain rates and falling snow. An example of ongoing work demonstrating the GPM-CO multi-instrument active/passive microwave, multi-frequency synergy is shown in Grecu *et al.* (2016) where the precipitation estimates from the combined DPR+GMI CORRA algorithm compared to ground validation data have good correlations but show room for improvement in future versions. Over land, advances have been made by the GPM GPROF algorithm through using GPM ground-validation datasets collected over the U.S. to adjust the GPROF V05 precipitation estimates over snow covered land surfaces. As a result of the GPROF algorithm modification, improvements were noted in GPROF V05 snowfall estimates based on independent comparisons to GV estimates made over the northern mid-latitude continental region of Hyytiälä, Finland (von Lerber *et al*., 2017).

The third step of the transfer standard uses the combined DPR and GMI CORRA estimates of the GPM-CO to provide a routinely updated calibration for all sensors in the GPM constellation before they are incorporated into the IMERG combined-satellite product. IR-based precipitation estimates used in IMERG are routinely calibrated by the collection of inter-calibrated passive microwave-based precipitation estimates. These two actions ensure that all

satellite precipitation estimates used in IMERG have a calibration traceable back to the CORRA product.

3.2 Contributions to water cycle understanding

Since launch, the DPR 3D measurements, detailed constellation observations, and the IMERG high spatial and temporal resolution merged-data products have provided data on the space-time variability of global precipitation used for scientific research. For example, Liu and Zipser (2015) collected the first year of GPM Ku radar data to classify the largest, deepest, and strongest precipitation systems on Earth. Figure 6 shows the Liu and Zipser (2015) classifications, updated using three years of the Version 05 GPM products (released May 2017). With the higher latitude coverage of the GPM-CO, the DPR confirms that precipitating storm systems in the Great Plains of the U.S. and the Pampas in Argentina are among the most intense on Earth. The largest precipitation systems are found in the mid-latitude extratropical storm tracks, highlighting the role of front in the organization of these larger precipitation systems. Using the DPR dataset Battaglia *et al.* (2016a) found the first evidence of "ghost echoes" which correspond to areas of multiple scattering within the weak-echo regions typically observed by ground-based S-band radar in the vicinity of a tilted convective core of a tornadic supercell. Meanwhile, using GMI microwave polarimetric signals from the vertical and horizontal channels, Gong and Wu (2017) found that the radiative scattering of frozen particles is highly polarized in the upper troposphere throughout the tropics and mid-latitude jet regions, and hence indicate that the ice particles are horizontally oriented. GPM continues to uncover the diversity of phenomena that are both important scientifically and crucial to developing the best retrievals for understanding the water cycle.

3.3 Inputs to hydrological modelling

Downscaling high-resolution precipitation data and innovative hydrological modelling have helped advance predictions of precipitation-related high-impact natural hazard events (e.g., flood, drought, landslide, and hurricanes) and improve hydrological modelling and prediction. GPM and TRMM data have been used to improve quantitative precipitation estimation over land within the U.S. (e.g. Wen *et al.*, 2016; Kirstetter *et al.*, 2015) and internationally (e.g., Libertino *et al.*, 2016). Petkovic and Kummerow (2015) examined the sources of bias in the GMI product, while Tan *et al.* (2016a) compared error sources in IMERG attributable to individual instruments, finding (as expected) that the most reliable IMERG estimates originate from passive microwave estimates. An error model to quantify uncertainty in fine resolution precipitation products for satellite hydrology was proposed by Maggioni *et al.* (2014) and Wright *et al.* (2017). Lin *et al.* (2015) developed a framework for dynamical precipitation downscaling through assimilating 6-h National Centers for Environmental Prediction (NCEP) Stage IV data using the Weather Research and Forecasting (WRF) 4-dimensional (4D)-Varational system. This physically based downscaling methodology can be considered as a proof of concept for the downscaling of fine-scale GPM precipitation observations.

3.4 Efforts toward advancing climate models

Information from GPM's estimates of surface water flux inputs, cloud/precipitation microphysics, convective/stratiform separation, and latent heat release in the atmosphere has the potential for improved parameterization and initialization of climate models (Hagos *et al*., 2014).

Climate models, and their parameterizations within the models, can be verified with global precipitation products but care must be taken to address limitations and enforce quality control (Tapiador *et al*., 2017). Research using information based upon GPM observations are helping to advance climate and other models that require parameterizations for convection and cloud microphysics. For example, using GPM field campaign data, Adirosi *et al.* (2016) compared raindrop size distributions to modelled size distributions, Tao *et al.* (2013) investigated the diurnal structure of precipitation, while Iguchi *et al.* (2014) used cloud resolving models to study melting-layer structure in mixed-phase precipitation, and Colle *et al.* (2017) viewed the structure and evolution of warm frontal precipitation. Hill et al. (2016) used TRMM data, in conjunction with other satellite data sets, to confirm that the most modern global atmospheric reanalysis (ERA-Interim, produced by European Centre for Medium-Range Weather Forecasts [ECMWF] available from 1979) and global models tend to generate convection too early in the day with consequences for the release of latent heat in south west Africa. More opportunities for studies like this should be possible once GPM calibrates and reprocesses TRMM data, creating a multi-decade record of precipitation.

3.5 Support for improved weather forecasting

GPM's accurate and frequent measurements of precipitation-affected radiances and instantaneous precipitation rates together with quantitative error characterization have been assimilated into weather forecasting and data assimilation systems to improve 4D reanalysis, with the GPM-CO data being used operationally by the ECMWF (Geer *et al.*, 2017). Assimilating satellite observations from microwave imagers such as GMI in cloudy and precipitating regions provides critical constraints on atmospheric parameters in dynamically

391 sensitive regions and makes significant impacts on weather forecast accuracy. Kim *et al.* (2017)
392 describe a framework to assimilate GMI all-sky (including cloud and precipitation affected)
393 radiance data using a hybrid 4D-Ensemble Variational (EnsVar) analysis algorithm in the
394 Goddard Earth Observing System version 5 (GEOS-5) that will become part of NASA's Global
395 Modelling and Assimilation Office (GMAO)'s operational forecast system in 2018.
396 Zhang *et al.* (2017) have developed an ensemble data assimilation system for the NASA
397 Unified Weather Research and Forecasting (NU-WRF) model, which can optimally integrate the
398 information from high-resolution numerical model predictions and from GPM satellite data.
399 Because precipitation varies greatly in time and space, they have developed an estimation
400 method for forecast errors by using an ensemble of forecasts with optimal perturbations to the
401 initial states of, for instance, temperature, humidity, precipitation, and clouds. The analysis
402 shows an improved representation of monsoon precipitation and its interaction with atmospheric
403 dynamics over West Africa. This assimilation of precipitation-affected microwave radiances
404 impacts the distribution of precipitation intensity and the propagation of cloud-precipitation
405 systems of the African Easterly Jet (Zhang *et al.*, 2017). The Joint Center for Satellite Data
406 Assimilation (JCSDA) is currently testing how GMI data improve track forecasting for tropical
407 cyclones (Kirschbaum *et al.*, 2017; Pu and Yu, 2017).

408

409 **4. Ground validation activities and contributions to the GPM mission**

410 GPM GV mission contributions have focused on the collection of high-quality continental
411 scale reference precipitation rate, accumulation and multi-parameter radar datasets; the
412 development and operation of research grade multi-frequency polarimetric radar and
413 precipitation measurement network instrumentation for describing hydrometeor physical

414 characteristics; and the design and implementation of numerous field campaigns consisting of
415 coordinated satellite, ground, and airborne *in situ* and remote sensing data collections that
416 describe liquid, mixed, and ice-phase precipitation types from hydrometeor to satellite sampling
417 scales (Hou *et al*., 2014). Broadly speaking, these GV contributions have resulted in data suited
418 to long-term direct statistical comparisons between GPM and GV data (e.g., Kirstetter *et al*.,
419 2012, 2015; Petersen *et al*., 2016; Tan *et al*., 2016a,b), as well as datasets from short, more
420 highly targeted field campaigns designed to study precipitation processes and the physical
421 validation of GPM retrieval algorithms (as listed in Table IV).

422

423 **4.1 GV Ground Instrument Infrastructure**

424 GPM GV has established a world-class inventory of precipitation instrumentation.
425 Equipment developed and operated as part of this instrument suite include the NASA S-band
426 dual-polarization (NPOL) radar (Wolff *et al.*, 2014), the Ku-Ka band Dual-frequency Dual-
427 Polarimetric Doppler Radar (D3R; Vega *et al.*, 2014), numerous Micro Rain Radars (MRR-2;
428 Peters *et al*., 2002), Pluvio-2 weighing gauges, dense networks of (multiple) tipping bucket rain
429 gauges, snow imaging/measurement systems such as the Precipitation Imaging Package (PIP)
430 (e.g., Newman *et al.*, 2009; Tiira *et al.*, 2016), and autonomously operating Parsivel and 2D
431 Video Disdrometer (2DVD) networks (e.g., Tokay *et al.*, 2017). When not deployed for GPM-
432 related field campaigns, these instruments operate within the NASA Wallops Flight Facility
433 (WFF) network (or partner sites), with special emphasis placed on data collections during GPM-
434 CO overpasses.

435

436 **4.2 Direct GV Datasets**

437 Considering longer-term statistical validation of GPM satellite products, GV contributions to
438 the mission include two primary multi-parameter datasets (see https://gpm-gv.gsfc.nasa.gov/ for
439 access to these and other GV datasets):

440 *1) Validation Network (VN) Radar Data:* VN data consist of ~80 U.S. network, oceanic, and/or
441 other national/international research site-specific dual polarimetric (dual-pol) radars that
442 provide derived precipitation rate, DSD and hydrometeor type data that are footprint and
443 column volume-matched to GPM-CO overpasses (Bolen and Chandrasekar, 2003; Schwaller
444 and Morris, 2011). Over 41,000 GPM-VN radar volumes were processed between launch and
445 September 2017 and processing continues. Early VN datasets supported validation of TRMM
446 rainfall rates (e.g., Islam *et al*., 2012) and checks on surface radar calibration stability in
447 preparation for the GPM-era (e.g., Kim *et al*., 2014). In the GPM era the aforementioned types
448 of study, now using the DPR instead of TRMM's Precipitation Radar (PR) continue, but the
449 VN has also directly supported verification of mission science requirements (Petersen et al.
450 2017), DSD retrieval algorithms (e.g., Grecu *et al*., 2016), and even studies of GPM hail
451 detection (Leppert and Cecil, 2015).

452

453 *2) GV-Multi-Radar Multi-Sensor (MRMS) Precipitation Rates*: GV-MRMS data are rain gauge
454 bias-adjusted radar estimates of precipitation rate and type (rain/snow) for GPM products over
455 the U.S. and neighboring regions (130°-60°W, 20°-55°N). GV-MRMS datasets are derived
456 from NOAA MRMS products (Zhang *et al*., 2016), but are further processed (e.g., Kirstetter
457 *et al*., 2012) to produce gauge-corrected reference precipitation intensity datasets augmented
458 with information on precipitation types and data quality at the native temporal (2-minute) and

spatial resolution (0.01° x 0.01°) of the MRMS. These products have been used for statistical validation of instantaneous GPM precipitation estimates at individual IFOVs scales (e.g., Kidd *et al*., 2017b). GV-MRMS data are also used to create 30-minute rain accumulation datasets (including precipitation type, radar quality metrics, etc.) to validate IMERG products (e.g., Tan *et al*., 2016a,b) and have been integrated with IMERG and field data for hydrologic validation/assimilation studies (e.g., Tao *et al*., 2016).

4.3 GV Field Campaigns

GPM GV has implemented six major field campaigns (e.g., Figure 3; Table IV), has participated in several targeted international partner-led field campaigns, and conducts ongoing field measurements made at supersites such as WFF. The field measurements focus on a wide range of cold- and warm-season precipitation regimes. Associated datasets (Table IV) include virtually all of the aforementioned ground-based direct-statistical datasets discussed above, but also include high-altitude airborne combinations of radar (W, Ku, Ka, X-band frequencies) and passive microwave radiometer (e.g., 10-183 GHz) remote-sensing data collected from instruments on the NASA DC-8 and/or ER-2 aircraft, airborne *in situ* cloud microphysical measurements, and supporting sounding profiles of atmospheric thermodynamic state.

GV field measurements and related instruments connect GPM satellite-based remote sensing algorithms to column physical processes and precipitation measured at the Earth's surface. The associated data have supported a range of studies related to the testing, development, and/or verification of GPM retrieval algorithms and supporting cloud models. These include the physics of, and methods to parameterize, the DSD (e.g., Williams *et al*., 2014; Liao *et al*., 2014; Tokay *et al*., 2017; Raupach and Berne, 2017), including new observations of small raindrops (< 0.5 mm)

and their impact on current approaches to representing the DSD in light rain (Thurai *et al*., 2017), radar multiple-scattering at DPR frequencies in strong convection (Heymsfield *et al.*, 2013; Battaglia *et al.*, 2016a), and hail signatures in radiometer data (Leppert and Cecil, 2015). Examples of multi-frequency ice and snow scattering studies include Molthan and Petersen (2011), Tyynelä and Chandrasekar (2014), Kneifel *et al.* (2015), and Olson *et al.* (2016), while measurements of snow water equivalent rate can be found in Moisseev *et al.* (2017) and von Lerber *et al.* (2017). GPM's field campaign data have also supported cloud resolving model microphysics (e.g., Shi *et al.*, 2010; Tao *et al.*, 2013; Lang *et al.*, 2014; Colle *et al.*, 2017) and have combined the use of hydrologic modelling and observations to develop "best" estimates of liquid and frozen precipitation accumulation over complex terrain (Cao *et al*., 2017).

In late 2015 and early 2016, GPM GV completed a large field campaign over the mountainous region of the Olympic Peninsula of Washington State, US (OLYMPEX; Houze *et al*., 2017). In contrast to the warm-season Integrated Precipitation and Hydrology Experiment (IPHEx) campaign that focused primarily on orographic warm-season convective rain (e.g., Table IV), OLYMPEX focused on validation of GPM algorithms and products in cold-season mid-latitude frontal system precipitation (rain and snow) influenced by complex terrain. Indeed, heavy precipitation frequently occurred over the Olympic Mountains with several rain events exceeding 250 mm in 1-2 day time spans along windward slopes. Figure 7 provides one example sampled by ground-based radar, aircraft, and an overpass of the GPM-CO. As evident in Figure 7, orographic perturbation of the prevailing low-level flow and associated enhancements of the precipitation process were important during OLYMPEX (see also Houze *et al*., 2017, and Zagrodnik *et al*., 2017). In fact, Figure 7b suggests that orographic enhancements occurring below 2 km (Figs. 7c-d) may be difficult to directly observe using GPM DPR observations. If the

505 enhancement is associated with warm-rain processes, it may also be difficult for radiometers to
506 reliably detect (e.g., Shige and Kummerow, 2016). Indeed, Cao *et al*. (2017) used OLYMPEX
507 measurements and the Variable Infiltration Capacity (VIC) model to develop a composite
508 reference estimate of daily total rain and snow water equivalent at a spatial resolution of 1/32°
509 over the OLYMPEX domain for the October-April 2015-16 time period centered on the
510 experiment. When compared to this reference, it was found that both IMERG and GSMaP
511 underestimated the precipitation by approximately 50% over the higher terrain. From this
512 perspective, detailed analysis of OLYMPEX airborne and ground-based observations will be
513 useful for informing and/or verifying physical processes and estimation uncertainties in GPM
514 retrieval algorithms and associated products in similar frontal/orographic regimes.

515 Near-term international field efforts such as the International Collaborative Experiment –
516 PyeongChang Olympics-Paralympics 2018 (ICE-POP 2018; led by the Korean Meteorological
517 Administration, February-March, 2018) are enabling further GPM studies of orographic
518 precipitation processes, and in particular, orographic snow, over regions characterized by large
519 ocean to mountain terrain gradients. All GV field campaign datasets are openly available via the
520 Global Hydrology Resource Center Distributed Active Archive Center (DAAC) located at
521 NASA Marshall Space Flight Center (MSFC) (https://ghrc.nsstc.nasa.gov/home/field-campaigns).

522

523 **5. Applications of GPM data for societal benefit**

524 GPM data provide critical information to end-users that helps to improve our understanding of
525 Earth's water cycle and facilitates decision-making at local to global scales (Kirschbaum *et al.*,
526 2017). Building on the legacy of TRMM, the use of high-quality precipitation data provided by

GPM, now covering higher latitudes, has enabled new science research and data applications to benefit society across a diverse range of end-users; some examples are shown in Table V and summarized below.

5.1 Hydrologic modelling, prediction, and water resource management

GPM's instantaneous precipitation products, especially IMERG, are being used as input into hydrological and land surface models. Short-term forecasts of soil moisture and other parameters to better understand the land-atmosphere interactions on scales of days to years are available from the NASA Land Information System (LIS, Kumar *et al.*, 2006) based on GPM and other precipitation data. LIS runs operationally providing data to forecasters in NRT through NASA's Short-term Prediction Research and Transition Center (SPoRT) and SERVIR (Spanish *to serve*) projects (https://weather.msfc.nasa.gov/sport/, https://www.servirglobal.net/).

TRMM and GPM data are being integrated with other rainfall forcing data into the multi-agency, multi-national Famine Early Warning System Network (FEWS NET; https://www.fews.net/). IMERG data have been tested within the FEWS NET Land Data Assimilation System to provide information on different agricultural products including the start of the growing season and drought metrics (Kirschbaum *et al.*, 2017). IMERG data have been connected with water resource managers and farmers in the Indus valley though the use of cellphone updates to farmers about when to irrigate their crops (Hossain *et al.*, 2017). GPM has also been important in contributing to food-water-energy dialogues (Shepherd *et al.*, 2016). GPM scientists have analyzed the distribution of the mean precipitation per person (PPP) using IMERG and population density estimates (Figure 8), which highlights the potential water

549 availability and potential water availability stressors coming purely from precipitation (Shepherd
550 *et al.*, 2016). High values are found in areas such as the Amazon basin, western U.S., and
551 Australia, where high precipitation but low populations exist, while areas with dense population,
552 including China and India, have lower PPP. This PPP dataset could lead to several interesting
553 studies such as: Do precipitation regimes (e.g., orographic) affect human habitability? How well
554 can high PPP areas support low PPP areas through water management, agriculture, and/or energy
555 production? What are the direct and indirect costs of these imbalances in global PPP?
556

557 **5.2 Operational numerical weather and hurricane prediction**

558 To facilitate early use of the GPM-CO data, an informal Early Adopter Program was
559 instituted during the GPM-CO's pre-launch and checkout phases. This early data access allowed
560 the Navel Research Lab (NRL) Automated Tropical Cyclone Forecasting System
561 (https://www.nrlmry.navy.mil/TC.html) to begin integrating GMI data into their system to
562 improve tropical cyclone location fixes the day after the data were released in June 2014 (3
563 months earlier than planned). As a result, GPM data were used to support tropical cyclone
564 forecasts from the start of the 2014 Atlantic Hurricane season. From June 2014-October 2017,
565 the NRL Tropical Cyclone webpage has recorded nearly 5,000 GMI overpasses of cyclones that
566 have been used by forecasters around the globe to monitor tropical cyclone structure (Dr. Song
567 Yang, personal communication). The GPM-CO DPR provided (3D) data during overpasses of
568 the 2017 Atlantic Hurricane season including the hot towers associated with Hurricanes Harvey,
569 Irma, Jose, Maria, and Ophelia (https://pmm.nasa.gov/extreme-weather/). In addition, GMI data
570 were specifically mentioned in NOAA's National Hurricane Center (NHC) hurricane forecasts
571 for Irma and Jose (National Hurricane Center, 2017). IMERG has been used to create rainfall

572 accumulation maps from many of the Atlantic (and worldwide) severe storms (e.g.,
573 https://svs.gsfc.nasa.gov/4586).

574 GMI Tb products are operationally assimilated into Numerical Weather Prediction (NWP)
575 models across the globe to improve short- to long-term weather forecasts and correct the track
576 forecasts for tropical cyclones. The Air Force Weather Agency (557th Weather Wing)
577 incorporates GMI data into their WRF model, delivering operational worldwide weather
578 products to the Army and Air Force, unified commands, National Programs, and the National
579 Command Authorities. The JCSDA/NOAA and ECMWF are working to use GPM-CO data
580 within their global NWP model focusing on medium-range (up to two weeks ahead) forecasts;
581 operational inclusion of GPM data into GEOS-5 is expected in 2018. GPM data are also accessed
582 daily by weather prediction agencies around the world including Japan, India, China, Korea,
583 Australia, United Kingdom, France, Brazil, Argentina, Netherlands, among others.

584 In partnership with the MSFC SPoRT Center, GPM single-channel and multispectral
585 radiometer imagery and rain rate products from all of the satellites in the GPM Constellation are
586 provided to the NHC in a format compatible with their operational National Center for
587 Environmental Prediction (NCEP) Advanced Weather Interactive Processing System (N-
588 AWIPS) decision support system. The satellite liaison at the NHC has confirmed that these data
589 are being ingested into the NHC from SPoRT and noted that integration of the suite of passive
590 microwave imagery (including the GPM-CO) into N-AWIPS has been one of the most
591 significant dataset additions in recent years (Chris Landsea, NHC, personal communication via
592 NASA's SPoRT facility).

593

5.3 Disaster response, extremes, and disease

Extreme precipitation leading to flood or landslide events, and the characterization of potential hazards, are a source of several GPM investigations (e.g., Petkovic and Kummerow, 2015; Panegrossi *et al.*, 2016; Kirschbaum *et al.*, 2015b). The IMERG spatial and temporal resolutions provide a valuable product to examine precipitation extremes that may result in flooding, landslides, or other meteorologically-induced phenomena and to support disaster response and recovery (Schumann *et al.*, 2016). TRMM and now GPM data are being used in the development and NRT processing of a Global Flood Monitoring System (e.g., Wu *et al.*, 2014) that provides estimates of flood detection, intensity, streamflow, and inundation. Similar work has developed a regional and global Landslide Hazard Assessment model for Situational Awareness (LHASA) that leverage both the long-duration TRMM Multi-satellite Precipitation Analysis (TMPA; Huffman *et al.*, 2007) data and IMERG to provide estimates of potential landslide activity around the world in NRT, as well as to evaluate the coincidence of global landslide data and extreme rainfall patterns (Kirschbaum *et al.*, 2015a). Figure 9 highlights the global distribution of average annual potential landslide activity, which can be used to improve situational awareness of landslide occurrence both spatially and temporally, especially in areas with few ground based observations. The LHASA model is now being run using the Early Run IMERG data (Table III) to provide NRT landslide nowcasts every 30 minutes at 0.1˚ resolution (available at https://pmm.nasa.gov/precip-apps). IMERG estimates are also being used within the Global Fire WEather Database (GFWED), which integrates different weather factors influencing the likelihood of the initiation and spreading of vegetation fires (Field *et al.*, 2015).

In areas where few rain gauges exist, monitoring or forecasting conditions that can lead to disease vector or water-borne diseases is extremely challenging. Consequently, satellite

precipitation estimates, often in NRT, are increasingly becoming the standard precipitation data source in these environments. The IMERG NRT data have been used to track environmental conditions on the ground in order to help predict and validate the risk of cholera infection, for example, as shown in Figure 10 for Haiti immediately after Hurricane Matthew in October, 2016 (Khan *et al.*, 2017). Studies using TRMM have shown that areas of wetter conditions in the higher elevations of Uganda are often associated with increased incidence of Black Plague (Monaghan *et al.*, 2012; MacMillan *et al.*, 2012). TRMM and GPM estimates are also being used to characterize mosquito-breeding habitats in an effort to identify areas with higher disease risk (Valle *et al.*, 2013; Pan *et al.*, 2014; Zaitchik *et al.*, 2014). Research applications will improve with GPM's increased spatiotemporal resolution and accuracy, helping to improve the environmental and climatic conditions for increased disease outbreaks.

6. Conclusions and future prospects

The GPM-CO has proven to be a worthy successor to TRMM, extending and improving high-quality active and passive microwave observations across all times of day with a precessing 65°-inclination orbit. The GPM-CO has provided new insights into sensing snowfall as well as continued innovation across the range of precipitation systems from the Arctic to the Antarctic Circle. The GPM-CO has met its mission success metrics, has set a new standard for passive microwave radiometer accuracy, and has provided the data for processing and disseminating precipitation data for a range of scientific investigations and societal applications. The GPM mission also has provided leadership and the calibration transfer standard (via the GPM-CO) to unify and advance precipitation measurements from a constellation of research and operational sensor data shared by a consortium of domestic and international partners.

640 The GPM mission is currently in extended operations after successfully completing its end of
641 prime mission review in June 2017 after 3 years on orbit. The GPM-CO has fuel onboard that
642 could last for more than a decade, which provides significant opportunities to continue to
643 maximize the scientific and societal benefits of the mission (contingent on instrument health) by
644 enhancing the understanding of precipitation physical character, processes, structure, and
645 variability from regional to global scales and sub-daily to interannual scales.

646 In terms of algorithm and products for extended operations, the mission seeks to address the
647 following major topics: lengthen the temporal record by inter-calibrating datasets back to 1998
648 (for the complete TRMM record, expected release in 2018), extend GPM merged constellation
649 algorithms pole to pole and improve their morphing process, and improve the estimates of falling
650 snow and light rainfall. One critical issue is to improve spaceborne estimates of precipitation
651 over orographic and other complex surface features. In addition, the effects of multiple scattering
652 and non-uniform filling of footprints by precipitation have not been fully addressed in
653 simulations of radar reflectivities in the DPR and CORRA algorithms, although improved
654 parameterizations are being developed. These effects greatly impact the interpretation of DPR
655 observations at Ka- and Ku-bands.

656 Scientifically, an extended GPM mission will help to determine inter-annual spatial and
657 temporal variability of global rainfall, hydrometeor and microphysical structure, and associated
658 latent heating for convective systems and storms, and how these characteristics are related to
659 variations in the global water and energy cycles. The longer precipitation record will increase our
660 knowledge of mean precipitation variations and intensity distributions from inter-annual to
661 multi-decadal time scales by utilizing the increased sampling statistics, accuracy, and
662 passive/active synergy of the GPM and TRMM observations, by linking this recent period to

663 earlier observations and by validating modelling results from emerging high-resolution climate
664 models.

665 New GPM science investigations fall into the following themes: (1) research on microphysics
666 and physical properties of precipitation systems observed by the GPM-CO, including the
667 characterizations of extreme events; (2) long-term precipitation datasets that will permit global
668 precipitation and circulation pattern investigations, including their variability in terms of ENSO
669 and other global time variations; and (3) the development of fine-scale regional climatologies of
670 precipitation characteristics (mean surface rain, diurnal cycle, vertical structure) on a monthly to
671 seasonal basis. Through assimilation and other methods, the U.S. GPM project plans to develop a
672 national precipitation product based on modelling that reproduces GPM precipitation statistics at
673 the time and space scales of the observations, but also defines higher resolution (downscaled)
674 information for scientific studies and applied uses.

675 New research might include studies of other retrievable products (such as winds and surface
676 emissivity) from the GPM datasets, more detailed estimates of latent heating in the mid-latitudes,
677 improved estimates of light rain, and better assessments of falling snow properties. Early work
678 has shown that ocean wind speeds are retrievable from GPM data (Munchak *et al.*, 2016;
679 Nouguier *et al.*, 2016) but require verification through additional scientific investigations and
680 validation efforts. Enhancement of land and ocean surface emissivity/radar cross section
681 retrievals (e.g., Prigent *et al.*, 2015; Tian *et al.*, 2013; Ferraro *et al.*, 2013; Harrison *et al.*, 2016;
682 Turk *et al.* 2014) is important because these are vital environmental conditions required by the
683 precipitation retrieval algorithms, especially as the algorithms move toward more physically
684 based descriptions of surface properties (e.g., Kummerow *et al.*, 2015). Other research in process
685 involves extending the TRMM Latent Heating dataset to the mid-latitudes, where the

686 organization of mid-latitude cyclones is vastly different than that of convective systems in the
687 tropics (Liu and Liu, 2016; Liu and Zipser, 2015). Scientific investigations are required to assess
688 the differences of latent heat structure in stratiform and convective precipitation regions in the
689 mid-latitudes, and to address what defines these structures at these latitudes.

690 TRMM has shown the value of a long record of precipitation in many science inquiries (e.g.,
691 Curtis *et al.*, 2007; Lau and Wu, 2010; Liu *et al.*, 2015). GPM will expand this record and, in
692 addition, because of the increased mid-latitude coverage of the GPM-CO compared to TRMM,
693 scientific investigations are planned for these higher latitudes. For example, the GPM-CO can
694 now track tropical cyclones as they become extra-tropical and can help identify corresponding
695 changes in precipitation characteristics as storm structure changes at higher latitudes and permits
696 coordinated observational and modelling studies on storm intensity and precipitation. The GPM-
697 CO is the first NASA satellite capable of measuring moderate and heavy snowstorms in detail. In
698 particular, the 3D capabilities of DPR bring new space-based capabilities for studying classical
699 Nor'easters and other extratropical storms in the northern or southern hemispheres.

700 A key contribution to the community will be the retrospective processing of the U.S. team's
701 IMERG back to 2000, which will be released to the public in 2018. These datasets will provide
702 the first-ever fine-scale record of quasi-global precipitation for nearly two decades computed
703 with the next-generation GPM-based algorithms. Continued computation of near-real-time and
704 high quality research estimates will benefit society though improvement across a range of
705 application and operational activities, including storms, floods, landslides, droughts, agricultural
706 forecasting, and water resource management. Taken together, these initiatives will continue to
707 exploit the potential of the GPM-CO and constellation to advance precipitation science and
708 address societal needs in the coming years. Indeed, GPM's precipitation observations are key to

addressing World Climate Research Program (WCRP) research challenges by providing data for scientific studies such as improving our knowledge of atmospheric circulation patterns, defining precipitation's role in climate sensitivity, cataloging weather extremes, assessing precipitation inputs for the world's agricultural food baskets, and providing key observations that refine modelling assumptions about precipitation, thus improving climate prediction.

7. Acknowledgements

Thanks go to Lisa Milani (National Research Council of Italy/Michigan Technical University) for the CloudSat/DPR difference images of Figure 5; Stephanie Wingo (NASA MSFC/USRA) for contributions to Figure 7; Chuntao Liu (Texas A&M) and Marshall Shepherd (University of Georgia) for Figure 8, and Antar Jutla (West Virginia University) for Figure 10. Thanks also go to, Pierre Kirstetter (NOAA/National Severe Storms Laboratory) for MRMS processing and related research, and Lisa Nalborczyk (NASA Goddard Space Flight Center) for helping with editing. Our three anonymous reviewers provided valuable feedback. We also thank NASA's Precipitation Measurement Mission science team and international partners (https://pmm.nasa.gov/PMM-science-team), as well as the international GV teams for their excellent support.

8. References

Adirosi E, Volpi E, Lombardo F, Baldini L, 2016. Raindrop size distribution: Fitting performance of common theoretical models. *Adv. Water Res.* 96 : 290 - 305. DOI: 10.1016/j.advwatres.2016.07.010

Aonashi K, Awaka J, Hirose M, Kozu T, Kubota T, Liu GS, Shige S, Kida S, Seto S, Takahashi N, Takayabu, YN, 2009. GSMaP Passive Microwave Precipitation Retrieval Algorithm: Algorithm Description and Validation. *J. Meteorol. Soc. Japan*. 87A : 119 - 136. DOI: 10.2151/jmsj.87A.119

Arndt DS, Baringer MO, Johnson MR. 2010. State of the climate in 2009. *Bull. Amer. Meteor. Soc.* 91 : s1 – s222. DOI: 10.1175/BAMS-91-7-StateoftheClimate

Barros AP, Petersen W, Schwaller M, Cifelli R, Mahoney K, Peters-Liddard C, Shepherd M, Nesbitt S, Wolff D, Heymsfield G, Starr D. 2014. NASA GPM-Ground Validation: Integrated Precipitation and Hydrology Experiment 2014 Science Plan. EPL/Duke University (Pub.): 64pp.

http://dx.doi.org/10.7924/G8CC0XMR

Battaglia A, Mroz K, Tanelli S, Tridon F, Kirstetter PE. 2016a. Multiple-Scattering-Induced "Ghost Echoes" in GPM DPR Observations of a Tornadic Supercell. *J. Appl. Meteor. Climatol.* 55 : 1653 - 1666. DOI: 10.1175/JAMC-D-15-0136.1

Battaglia A, Mroz K, Lang T, Tridon F, Tanelli S, Tian L, Heymsfield GM. 2016b. Using a multiwavelength suite of microwave instruments to investigate the microphysical structure of deep convective core. *J. Geophys. Res.* 121 : 9356 - 9381. DOI: 10.1002/2016JD025269

Battaglia A, Tanelli S, Mroz K, Tridon F, 2015. Multiple scattering in observations of the GPM dual-frequency precipitation radar: Evidence and impact on retrievals. *J. Geophys. Res.* 120 : 4090 - 4101. DOI: 10.1002/2014JD022866

Battaglia A, Tanelli S, Heymsfield GM, Tian L. 2014. The Dual Wavelength Ratio Knee: A Signature of Multiple Scattering in Airborne Ku–Ka Observations. *J. Appl. Meteor. Climatol*. 53 : 1790 – 1808. DOI: 10.1175/JAMC-D-13-0341.1

Berg W, Bilanow S, Chen R, Datta S, Draper D, Ebrahimi H, Farrar S, Jones WL, Kroodsma R, McKague D, Payne V, Wang J, Wilheit T, Yang JX. 2016. Intercalibration of the GPM Radiometer Constellation. *J. Atmos. Oceanic Technol.* 33 : 2639 – 2654. DOI: 10.1175/JTECH-D-16-0100

Bolen S, Chandrasekar V. 2003. Methodology for aligning and comparing spaceborne radar and ground-based radar observations. *J. Atmos. Oceanic Technol*. 20 : 647 – 659. DOI: 10.1175/1520-0426(2003)20<647:MFAACS>2.0.CO;2

Cao, Q., Painter, T. H., Currier, W. H., Lundquist, J. D., Lettenmaier, D. P., 2017: Estimation of precipitation over the OLYMPEX domain during winter 2015-16. *J. Hydrometeor.,* accepted.

Casella D, Panegrossi G, Sanò P, Marra AC, Dietrich S, Johnson BT, Kulie MS. 2017. Evaluation of the GPM-DPR Snowfall Detection Capability: Comparison with CloudSat-CPR. *Atmos. Res*. 197 : 64 – 75. DOI: 10.1016/j.atmosres.2017.06.018

Chambon P, Zhang SQ, Hou AY, Zupanski M, Cheung S. 2014. Assessing the impact of pre-GPM microwave precipitation observations in the Goddard WRF ensemble data assimilation system. *Quart. J. Roy. Meteorol. Soc.* 140 : 1219 – 1235. DOI: 10.1002/qj.2215

Colle BA, Naeger AR, Molthan A. 2017. Structure and Evolution of a Warm Frontal Precipitation Band during the GPM Cold Season Precipitation Experiment (GCPEx). *Mon. Wea. Rev.* 145 : 473 - 493. DOI: 10.1175/MWR-D-16-0072.1

Curtis S, Salahuddin A, Adler RF, Huffman GJ, Gu G, Hong Y. 2007. Precipitation Extremes Estimated by GPCP and TRMM: ENSO Relationships. *J. Hydromet.* 8 : 678 - 689. DOI: 10.1175/JHM601.1

Draper, DW, Newell DA, Wentz FJ, Krimchansky S, Skofronick-Jackson S. 2015a. The Global Precipitation Measurement (GPM) Microwave Imager (GMI): Instrument Overview and Early On-orbit Performance. *IEEE Journal of Selected Topics in Applied Earth Observations and Remote Sensing*. 8 : 3452 - 3462. DOI: 10.1109/JSTARS.2015.2403303

Draper, DW, Newell DA, McKague DS, Piepmeier JR. 2015b. Assessing Calibration Stability Using the Global Precipitation Measurement (GPM) Microwave Imager (GMI) Noise Diodes. *IEEE Journal of Selected Topics in Applied Earth Observations and Remote Sensing*. 8 : 4239 - 4247. DOI: 10.1109/JSTARS.2015.2406661

Ferraro R, Peters-Lidard CD, Hernandez C, Turk FJ, Aires F, Prigent C, Lin X, Boukabara SA, Furuzawa FA, Gopalan K, Harrison KW, Karbou F, Li L, Liu C, Masunaga H, Moy L, Ringerud S, Skofronick-Jackson GM, Tian Y, Wang NY. 2013. An Evaluation of Microwave Land Surface Emissivities over the Continental United States to Benefit GPM-Era Precipitation Algorithms. *IEEE Trans. Geoscience and Remote Sensing (TGARS)*. 51 : 378 - 398. DOI: 10.1109/TGRS.2012.2199121

Field, PR, Heymsfield AJ. 2015. Importance of snow to global precipitation. *Geophys. Res. Lett.* 42 : 9512–9520. DOI:10.1002/2015GL065497. http://dx.doi.org/10.1002/2015GL065497.

Field RD, Spessa AC, Aziz NA, Camia A, Cantin A, Carr R, De Groot WJ, Dowdy AJ. 2015. Development of a Global Fire Weather Database. *Nat. Hazards Earth Syst. Sci.* 15 : 1407 - 1423. DOI: 10.5194/nhess-15-1407-2015

Geer AJ, Baordo F, Bormann N, Chambon P, English SJ, Kazumori M, Lawrence H, Lean P, Lonitz K, Lupu C. 2017. The growing impact of satellite observations sensitive to humidity, cloud and precipitation. Q. J. R. Meteorol. Soc. DOI: 10.1002/qj.3172

Gong J, Wu DL. 2017. Microphysical Properties of Frozen Particles Inferred from Global Precipitation Measurement (GPM) Microwave Imager (GMI) Polarimetric Measurements. *Atmos. Chem. Phys.* 17 : 2741 - 2757. https://doi.org/10.5194/acp-17-2741-2017

Grecu M, Olson WS, Munchak SJ, Ringerud S, Liao L, Haddad Z, Kelley BL, McLaughlin SF. 2016. The GPM Combined Algorithm. *J. Atmos. Oceanic Technol.* 33 : 2225 - 2245. DOI: 10.1175/JTECH-D-16-0019.1

Hagos S, Feng Z, Burleyson CD, Lim K-SS, Long CN, Wu D, and Thompson G 2014: Evaluation of convection-permitting model simulations of cloud populations associated with the Madden-Julian Oscillation using data collected during the AMIE/DYNAMO field campaign, J. Geophys. Res. Atmos., **119**, 12,052–12,068, doi:10.1002/2014JD022143.

Hamada A, Takayabu YN. 2016. Improvements in Detection of Light Precipitation with the Global Precipitation Measurement Dual-Frequency Precipitation Radar (GPM DPR). *J. Atmos. Oceanic Technol.* 33 : 653 - 667. DOI: 10.1175/JTECH-D-15-0097.1

Harrison KW, Tian Y, Peters-Lidard C, Ringerud S, Kumar SV. 2016. Calibration to Improve Forward Model Simulation of Microwave Emissivity at GPM Frequencies Over the U.S.

Southern Great Plains. *IEEE Transactions on Geoscience and Remote Sensing*. 54 : 1103 - 1117. DOI: 10.1109/TGRS.2015.2474120

Heymsfield GM, Tian L, Li L, McLinden M, Cervantes JI. 2013. Airborne Radar Observations of Severe Hailstorms: Implications for Future Spaceborne Radar. *J. Appl. Meteor. Climatol*. 52 : 1851 – 1867. DOI: 10.1175/JAMC-D-12-0144.1

Hill PG, Allan RP, Chiu JC, Stein THM. 2016. A multisatellite climatology of clouds, radiation, and precipitation in southern West Africa and comparison to climate models. *J. Geophys. Res.* 121 : 10,857 - 10,879. DOI: 10.1002/2016JD025246

Hossain, F., N. Biswas, M. Ashraf, and B. A. Zeeshan, 2017: Growing More with Less in the Indus Valley Using Cellphones and Satellite Data. *Eos*. 98 : 1 - 12, https://doi.org/10.1029/2017EO075143

Hou AY, Kakar RK, Neeck S, Azarbarzin AA, Kummerow CD, Kojima M, Oki R, Nakamura K, Iguchi T. 2014. The Global Precipitation Measurements Mission. *Bull. Amer. Meteor. Soc.* 95 : 701 - 722. DOI: 10.1175/BAMS-D-13-00164.1

Houze, RA, McMurdie L, Petersen WA, Schwaller, MR, Baccus W, Lundquist J, Mass C, Nijssen B, Rutledge SA, Hudak D, Tanelli S, Mace GG, Poellot M, Lettenmaier D, Zagrodnik J, Rowe A, DeHart J, Madaus L, Barnes H. 2017. The Olympic Mountains Experiment (OLYMPEX). *Bull. Amer. Meteorol. Soc.* DOI: 10.1175/BAMS-D-16-0182.1

Huffman, GJ, Adler RF, Bolvin DT, Gu G, Nelkin EJ, Bowman KP, Hong Y, Stocker EF, Wolff DB. 2007. The TRMM Multi-satellite Precipitation Analysis: Quasi-Global, Multi-Year, Combined-Sensor Precipitation Estimates at Fine Scale. *J. Hydrometeor.* **8**: 38-55. DOI: 10.1175/JHM560

Huffman, GJ, Bolvin DT, Braithwaite D, Hsu K, Joyce R, Kidd C, Nelkin EJ, Sorooshian S, Tan J, Xie P. 2017. Algorithm Theoretical Basis Document (ATBD) Version 4.6 for the NASA Global Precipitation Measurement (GPM) Integrated Multi-satellitE Retrievals for GPM (I-MERG). 32pp. GPM Project: Greenbelt, MD. [Available online at https://pmm.nasa.gov/sites/default/files/document_files/IMERG_ATBD_V4.6.pdf]

Iguchi T, Seto S, Awaka J, Meneghini R, Kubota T, Chandra V, Yoshida N, Kawamoto N, Oki R. 2016. Precipitation rates estimated with GPM's Dual-frequency Radar. *Proc. IEEE Int. Conf. on Geoscience and Remote Sensing Symp. 2016*, *Beijing, China*, *10-15 July 2016*. 3917 - 3918pp. DOI: 10.1109/IGARSS.2016.7730017

Iguchi T, Matsui T, Tao WK, Khain AP, Phillips VTJ, Kidd C, L'Ecuyer T, Braun SA, Hou A. 2014. WRF–SBM Simulations of Melting-Layer Structure in Mixed-Phase: Precipitation Events Observed during LPVEx. *J. Appl. Meteor. Climatol*. 53 : 2710 - 2731. DOI: 10.1175/JAMC-D-13-0334.1

IPCC, 2014: Climate Change 2014: Synthesis Report. Contribution of Working Groups I, II and

III to the Fifth Assessment Report of the Intergovernmental Panel on Climate Change [Core Writing Team, R.K. Pachauri and L.A. Meyer (eds.)]. IPCC, Geneva, Switzerland, 151 pp.

Islam T, Rico-Ramirez MA, Han D, Srivastava PK, Ishak AM. 2012. Performance evaluation of the TRMM precipitation estimation using ground-based radars from the GPM validation network. *J. Atmos. Solar. Terrestrial Phys*. 77 : 194 - 208. DOI: 10.1016/j.jastp.2012.01.001

Jensen, MP, Petersen WA, Bansemer A, Bharadwaj N, Carey LD, Cecil DJ, Collis SM, Del Geneio AD, Dolan B, Gerlach J, Giangrande SE, Heymsfield A, Heymsfield G, Kollias P, Lang TJ, Nesbitt SW, Neumann A, Poellot M, Rutledge SA, Schwaller M, Tokay A, Williams CR, Wolff DB, Xie S, Zipser EJ. 2016. The Midlatitude Continental Convective Clouds Experiment (MC3E). *Bull. Amer. Meteor. Soc.* 97 : 1667 - 1686. DOI: 10.1175/BAMS-D-14-00228.1

Khan R, Anwar R, Akanda A, McDonald MD, Huq A, Jutla A, Colwell R. 2017. Assessment of Risk of Cholera in Haiti following Hurricane Matthew. *American Journal of Tropical Medicine and Hygiene*. DOI: 10.4269/ajtmh.17-0048

Kidd C, Huffman GJ, Becker A, Skofronick-Jackson G, Kirschbaum D, Joe P, Muller C, 2017a. So, how much of the Earth's surface *is* covered by rain gauges? *Bull. Amer. Meteor. Soc.* 98 : 69 - 78. DOI: 10.1175/BAMS-D-14-00283.1

Kidd C, Tan J, Kirstetter P-E, Petersen WA, 2017b: Validation of the Version 05 Level 2 precipitation products from the GPM Core Observatory and constellation satellite sensors. *Q. J. R. Meteorol. Soc.* First Published: 4 December 2017. DOI: 10.1002/qj.3175

Kidd C, Dawkins E, Huffman G. 2013. Comparison of Precipitation Derived from the ECMWF Operational Forecast Model and Satellite Precipitation Datasets. *J. Hydrometeor*. 14 : 1463 - 1482. DOI: 10.1175/JHM-D-12-0182.1

Kim M, Todling R, Gelaro R. 2017. Assimilation of All-sky GPM Microwave Imager (GMI) radiance data in NASA GEOS-5 model. Part I: Implementation. *Mon. Wea. Rev.*, Accepted.

Kim J, Ou M, Park J, Morris KR, Schwaller MR, Wolff DB. 2014. Global Precipitation Measurement (GPM) Ground Validation (GV) Prototype in the Korean Peninsula. *J. Atmos. Oceanic Technol.* 31 : 1902 – 1921. DOI: 10.1175/JTECH-D-13-00193.1

Kim JE, Alexander MJ. 2013. Tropical Precipitation Variability and Convectively Coupled Equatorial Waves on Submonthly Time Scales in Reanalyses and TRMM. *J. Climate*. 26 : 3013 - 3030. DOI: 10.1175/JCLI-D-12-00353.1

Kirschbaum DB, Huffman GJ, Adler RF, Braun S, Garrett K, Jones E, McNally A, Skofronick-Jackson G, Stocker E, Wu H, Zaitchik BF. 2017. NASA's Remotely-sensed Precipitation: A Reservoir for Applications Users. *Bull. Am. Meteorol. Soc.* 98 : 1169 – 1184. DOI: 10.1175/BAMS-D-15-00296.1

Kirschbaum DB, Patel K. 2016. Precipitation data key to food security and public health. *EOS*,

[Available online at https://eos.org/meeting-reports/precipitation-data-key-to-food-security-and-public-health]

Kirschbaum D, Stanley T, Zhou Y. 2015a. Spatial and temporal analysis of a global landslide catalog. *Geomorphology*. 249 : 4 – 15. DOI: 10.1016/j.geomorph.2015.03.016

Kirschbaum DB, Stanley T, Simmons J. 2015b. A dynamic landslide hazard assessment system for Central America and Hispaniola. *Nat. Hazards Earth Syst. Sci.* 15 : 2257 – 2272. DOI: 10.5194/nhess-15-2257-2015

Kirstetter PE, Hong Y, Gourley JJ, Schwaller M, Petersen W, Cao Q. 2015. Impact of sub-pixel rainfall variability on spaceborne precipitation estimation: evaluating the TRMM 2A25 product. *Q. Journal of the Royal Met. Soc.* 141 : 953 – 966. DOI: 10.1002/qj.2416

Kirstetter P, Hong Y, Gourley JJ, Chen S, Flamig ZL, Zhang J, Schwaller M, Petersen W, Amitai E. 2012. Toward a framework for systematic error modelling of spaceborne precipitation radar with NOAA/NSSL ground radar-based National Mosaic QPE. *J. Hydrometeor.* 13 : 1285 – 1300. DOI: 10.1175/JHM-D-11-0139.1

Kneifel S, von Lerber A, Tiira J, Moisseev D, Kollias P, Leinonen J. 2015. Observed relations between snowfall microphysics and triple-frequency radar measurements: Triple frequency signatures of snowfall. *J. Geophys. Res*. 120 : 6034 – 6055. DOI: 10.1002/2015JD023156

Kubota T, Yoshida N, Urita S, Iguchi T, Seto S, Meneghini R, Awaka J, Hanado H, Kida S, Oki R. 2014. Evaluation of Precipitation Estimates by at-Launch Codes of GPM/DPR Algorithms Using Synthetic Data from TRMM/PR Observations. *IEEE Journal of Selected Topics in Applied Earth Observations and Remote Sensing*. 7 : 3931 – 3944. DOI: 10.1109/JSTARS.2014.2320960

Kubota T, Iguchi T, Kojima M, Liao L, Masaki T, Hanado H, Meneghini R, Oki R. 2016. A Statistical Method for Reducing Sidelobe Clutter for the Ku-Band Precipitation Radar on board the GPM Core Observatory. J. Atmos. Oceanic Technol. 33: 1413-1428. DOI:10.1175/JTECH-D-15-0202.1

Kucera PA, Ebert EE, Turk FJ, Levizzani V, Kirschbaum D, Tapiador FJ, Loew A, Borsche M. 2013. Precipitation from space: Advancing Earth system science. *Bull. Amer. Meteor. Soc.* 94 : 365 – 375. DOI: 10.1175/BAMS-D-11-00171.1

Kumar SV, Peters-Lidard CD, Tian Y, Houser PR, Geiger J, Olden S, Lighty L, Eastman JL, Doty B, Dirmeyer P, Adams J, Mitchell K, Wood EF, Sheffield J. 2006. Land Information System - An Interoperable Framework for High Resolution Land Surface Modelling. *Environ. Model. Softw.* 21 : 1402 – 1415, [Available online at www.sciencedirect.com]

Kummerow CD, Randel DL, Kulie M, Wang NY, Ferraro R, Munchak SJ, Petkovic V. 2015. The Evolution of the Goddard Profiling Algorithm to a Fully Parametric Scheme. *J. Atmos. Oceanic Technol.* 32 : 2265 -2280. DOI: 10.1175/JTECH-D-15-0039.1

Kummerow CD, Ringerud S, Crook J, Randel D, Berg W. 2011. An observationally generated *a-priori* database for microwave rainfall retrievals. *J. Atmos. Oceanic Technol.* 28 : 113 – 130. DOI: 10.1175/2010JTECHA1468.1

Kummerow C, Simpson J, Thiele O, Barnes W, Chang ATC, Stocker E, Adler RF, Hou A, Kakar R, Wentz F, Ashcroft P, Kozu T, Hong Y, Okamoto K, Iguchi T, Kuroiwa H, Im E, Haddad Z, Huffman G, Ferrier B, Olson WS, Zipser E, Smith EA, Wilheit TT, North G, Krishnamurti T, Nakamura K. 2000. The Status of the Tropical Rainfall Measuring Mission (TRMM) after Two Years in Orbit. *J. Appl. Meteorol.* 39 : 1965 – 1982. DOI: 10.1175/1520-0450(2001)040<1965:TSOTTR>2.0.CO;2

Kuo, KS, Olson WS, Johnson BT, Grecu M, Tian L, Clune TL, van Aartsen BH, Heymsfield AJ, Liao L, Meneghini R. 2016. The Microwave Radiative Properties of Falling Snow Derived from Nonspherical Ice Particle Models. Part I: An extensive database of simulated pristine crystals and aggregate particles, and their scattering properties, *J. Appl. Meteor. Climatol.* 55 : 691 – 708. DOI: 10.1175/JAMC-D-15-0130.1

Lau KM, Wu HT. 2010. Characteristics of precipitation, cloud, and latent heating associated with the Madden–Julian Oscillation. *J. Climate*. 23 : 504 – 518. DOI: 10.1175/2009JCLI2920.1

Leppert KD, Cecil DJ. 2015. Signatures of Hydrometeor Species from Airborne Passive Microwave Data for Frequencies 10–183 GHz. *J. Appl. Meteor. Climatol.* 54 : 1313 – 1334. DOI: 10.1175/JAMC-D-14-0145.1

Liao L, Meneghini R, Tokay A. 2014. Uncertainties of GPM DPR Rain Estimates Caused by DSD Parameterizations. *J. Appl. Meteor. Climatol.* 53 : 2524 – 2537. DOI: 10.1175/JAMC-D-14-0003.1

Libertino A, Sharma A, Kalshmi V, Claps P. 2016. A global assessment of the timing of extreme rainfall from TRMM and GPM for improving hydrologic design. *Environmental Research Letters,* 11 : 054003. DOI: 10.1088/1748-9326/11/5/054003

Lin LF, Ebtehaj AM, Bras RL, Flores AN, Wang J. 2015. Dynamical Precipitation Downscaling for Hydrologic Applications Using WRF 4D-Var Data Assimilation: Implications for GPM Era. *J. Hydrometeor.* 16 : 811 – 829. DOI: 10.1175/JHM-D-14-0042.1

Liu C, Shige S, Takayabu Y, Zipser E. 2015. Latent Heating Contribution from Precipitation Systems with Different Sizes, Depths, and Intensities in the Tropics. *J. Climate*. 28 : 186 – 203. DOI: 10.1175/JCLI-D-14-00370.1

Liu C, Zipser EJ. 2015. The global distribution of largest, deepest, and most intense precipitation systems. *Geophys. Res. Lett.* 42 : 3591 – 3595. DOI: 10.1002/2015GL063776

Liu C, Zipser EJ. 2009. "Warm Rain" in the tropics: seasonal and regional distributions based on 9 yr. of TRMM data. *J. Climate*. 22 : 767 – 779. DOI: 10.1175/2008JCLI2641.1

Liu N, Liu C. 2016. Global distribution of deep convection reaching tropopause in 1 year GPM observations. *J. Geophys. Res.* 121 : 3824 – 3842. DOI: 10.1002/2015JD024430

Liu WT, Xie X. 2017. Pre-monsoon drought in India observed from space. *J. of Hydrometeor.* 18 : 683 – 692. DOI: 10.1175/JHM-D-16-0014.1

MacMillan K, Monaghan AJ, Apangu T, Griffith KS, Mead PS, Acayo S, Acidri R, Moore SM, Mpanga JT, Enscore RE, Gage KL, Eisen RJ. 2012. Climate predictors of the spatial distribution of human plague cases in the West Nile region of Uganda. *Am. J. Trop. Med. Hyg.* 86 : 514 – 523. DOI: 10.4269/ajtmh.2012.11-0569

Maggioni V, Sapiano MRP, Adler RF, Tian Y, Huffman GJ. 2014. An Error Model for Uncertainty Quantification in High-Time-Resolution Precipitation Products. *J. Hydrometeor.* 15 : 1274 – 1292. DOI: 10.1175/JHM-D-13-0112.1

Masaki T, Kubota T, Oki R, Furukawa K, Kojima M, Miura T, Iguchi T, Hanado H, Kai H, Yoshida N, Higashiuwatoko T. 2015. Current status of GPM/DPR level 1 algorithm development and DPR calibration. *Proc. IEEE Int. Conf. on Geoscience and Remote Sensing Symp. 2015, Milan, Italy*. 2615 – 2618. DOI: 10.1109/IGARSS.2015.7326348.

Moisseev D, von Lerber A, Tiira J. 2017. Quantifying the effect of riming on snowfall using ground-based observations. *J. Geophy. Res. Atmos*. 122 : 4019 – 4037 DOI: 10.1002/2016JD026272

Molthan A, Petersen WA. 2011. Incorporating Ice Crystal Scattering Databases in the Simulation of Millimeter Wavelength Radar Reflectivity. *J. Atmos. Ocean Tech*. 26 : 2257 – 2269. DOI: 10.1175/2010JTECHA1511.1

Monaghan AJ, MacMillan K, Moore SM, Mead PS, Hayden MH, Eisen RJ. 2012. A regional climatography of West Nile, Uganda, to support human plague modelling. *J. Appl. Meteorol. Climatol.* 51 : 1201 – 1221. DOI: 10.1175/JAMC-D-11-0195.1

Munchak SJ, Meneghini R, Grecu M, Olson WS. 2016. A Consistent Treatment of Microwave Emissivity and Radar Backscatter for Retrieval of Precipitation over Water Surfaces. *J. Atmos. Oceanic. Technol.* 33 : 215 – 229. DOI: 10.1175/JTECH-D-15-0069.1

Munchak SJ, Skofronick-Jackson G. 2012. Evaluation of precipitation detection over various surfaces from passive microwave imagers and sounders. *Atmos. Res.* 131 : 81 – 94. DOI: 10.1016/j.atmosres.2012.10.011

National Hurricane Center, 2017. http://www.nhc.noaa.gov/archive/2017/al12/al122017.discus.024.shtml? http://www.nhc.noaa.gov/archive/2017/al11/al112017.discus.037.shtml? (accessed Nov 14, 2017)

National Research Council, 2013. *Climate and social stress: implications for security analysis*. National Academies Press.

Newman A, Kucera P, Bliven L. 2009. Presenting the Snowflake Video Imager (SVI). *J. Atmos. Oceanic Tech.* 26 : 167 – 179. DOI: 10.1175/2008JTECHA1148.1

Nouguier F, Mouche A, Rascle N, Chapron B, Vandemark D. 2016. Analysis of Dual-Frequency Ocean Backscatter Measurements at Ku- and Ka-Bands Using Near-Nadir Incidence GPM Radar Data. *IEEE Geoscience and Remote Sensing Letters*. 13 : 1310 – 1314. DOI: 10.1109/LGRS.2016.2583198

Olson WS, Tian L, Grecu M, Kuo KS, Johnson BT, Heymsfield AJ, Bansemer A, Heymsfield GM, Wang JR, Meneghini R. 2016. The Microwave Radiative Properties of Falling Snow Derived from Nonspherical Ice Particle Models. Part II: Initial Testing Using Radar, Radiometer and In Situ Observations. *J. Appl. Meteor. Climatol.* 55 : 709 – 722. DOI: 10.1175/JAMC-D-15-0131.1

Pan W, Branch O, Zaitchik B. 2014. Impact of climate change on vector-borne disease in the amazon. *Global Climate Change and Public Health*, Springer, New York. 7 : 193 – 210. DOI: 10.1007/978-1-4614-8417-2_11

Panegrossi G, Casella D, Dietrich S, Marra AC, Sanó P, Mugnai A, Baldini L, Roberto N, Adirosi E, Cremonini R, Bechini R, Vulpiani G, Petracca M, Porcù. 2016. Use of the GPM Constellation for Monitoring Heavy Precipitation Events Over the Mediterranean Region. *IEEE Journal of Selected Topics in Applied Earth Observations and Remote Sensing*. 9 : 2733 – 2753. DOI: 10.1109/JSTARS.2016.2520660

Peters, G., Fischer, B., T. Andersson, 2002: Rain observations with a vertically-looking Micro Rain Radar (MRR). *Boreal Env. Res*., **7**, 353-362.

Petersen WA, Houze RA, McMurdie L, Zagrodnik J, Tanelli S, Lundquist J, Wurmann J. 2016. The Olympic Mountains Experiment (OLMPEX): From Ocean to Summit. *Meteorol. Tech. Int'l.* Vol. Sept. 2016 : 22 – 26pp.

Petersen WA, Huffman G, Kidd C, Skofronick-Jackson G. 2017. Ground Validation Assessments of GPM Core Observatory Science Requirements. *European Geophysical Union, General Assembly, Vienna, Austria 23-28 April, 2017*.

Petkovic V, Kummerow CD. 2015. Performance of the GPM Passive Microwave Retrieval in the Balkan Flood Event of 2014. *J. Hydrometeor.* 16 : 2501 – 2518. DOI: 10.1175/JHM-D-15-0018.1

Prigent C, Liang P, Tian Y, Aires F, Moncet JL, Boukabara SA. 2015. Evaluation of modelled microwave land surface emissivities with satellite-based estimates. *J. Geophys. Res.* 120 : 2706 – 2718. DOI: 10.1002/2014JD021817

Pu, Z. and C. Yu. 2017. Assimilation of GPM Microwave Imager Clear-Sky Radiance in improving Hurricane Forecasts. Joint Center for Satellite Data Assimilation Quarterly, No. 57, https://doi.org/10.7289/V50P0X8R

Rasmussen R, Baker B, Kochendorfer J, Meyers T, Landolt S, Fischer AP, Black J, Thériault JM, Kucera P, Gochis D, Smith C, Nitu R, Hall M, Ikeda K, Gutmann E. 2012. How Well Are We Measuring Snow: The NOAA/FAA/NCAR Winter Precipitation Test Bed. *Bull. Amer. Meteor. Soc.* 93 : 811 – 829. DOI: 10.1175/BAMS-D-11-00052.1

Raupach T, Berne A. 2017. Invariance of the double-moment normalized raindrop size distribution through 3D spatial displacement in stratiform rain. *J. Appl. Meteorol. Clim*. 56 : 1663 - 1680. DOI: 10.1175/JAMC-D-16-0316.1

Reed PM, Chaney NW, Herman JD, Ferringer MP, Wood EF. 2015. Internationally coordinated multi-mission planning is now critical to sustain the space-based rainfall observations needed for managing floods globally. *Environ. Res. Lett.* 10 : 024010. DOI: 10.1088/1748-9326/10/2/024010

Schäfer SAK, Hogan RJ, Klinger C, Chiu JC, Mayer B. 2016. Representing 3-D cloud radiation effects in two-stream schemes: 1. Longwave considerations and effective cloud edge length. *J. Geophys. Res.* 121 : 8567 – 8582. DOI: 10.1002/2016JD024876

Schumann G, Kirschbaum D, Anderson E, Rashid K. 2016. *Role of Earth Observation Data in Disaster Response and Recovery: From Science to Capacity Building*. Earth Science Satellite Applications: Current and Future Prospects. F. Hossain, Ed., Springer Remote Sensing/Photogrammetry, Switzerland, 119–146

Schwaller MR, Morris KR. 2011. A Ground Validation Network for the Global Precipitation Measurement Mission. *J. Atmos. Oceanic Technol*. 28 : 301 – 319. DOI: 10.1175/2010JTECHA1403.1

Seto S, and Iguchi T. 2015. Intercomparison of Attenuation Correction Methods for the GPM Dual-Frequency Precipitation Radar. *J. Atmos. Oceanic Technol.* 32 : 915 – 926. DOI: 10.1175/JTECH-D-14-00065.1

Sims EM, Liu G. 2015. A Parameterization of the Probability of Snow-Rain Transition. *J. Hydrometeor.* 16 : 1466 – 1477. DOI: 10.1175/JHM-D-14-0211.1

Shepherd JM, Burian S, Liu C, Bernardes S. 2016. Satellite Precipitation Metrics to Study the Energy-Water-Food Nexus within the Backdrop of an Urbanized Globe. *Earthzine*. [Available online at http://earthzine.org/2016/05/31/satellite-precipitation-metrics-to-study-the-energy-water-food-nexus-within-the-backdrop-of-an-urbanized-globe]

Shi R, Tao WK, Matsui T, Cifelli R, Hou A, Lang S, Tokay A, Wang NY, Peters-Lidard C, Skofronick-Jackson G, Rutledge S, Petersen W. 2010. WRF Simulations of the 20-22 January 2007 Snow Events over Eastern Canada: Comparison with in-situ and Satellite Observations. *J.*

Appl. Meteor. Climatol. 49 : 2246 – 2266. DOI: 10.1175/2010JAMC2282.1

Shige, S. and Kummerow, CD. 2016. Precipitation-Top Heights of Heavy Orographic Rainfall in the Asian Monsoon Region. J. Atmos. Sci. 73:8, 3009-3024

Skofronick-Jackson G, Petersen WA, Berg W, Kidd C, Stocker EF, Kirschbaum DB, Kakar R, Braun SA, Huffman GJ, Iguchi T, Kirstetter PE, Kummerow C, Meneghini R, Oki R, Olson WS, Takayabu YN, Kurukawa K, Wilheit T. 2017. The Global Precipitation Measurement (GPM) Mission for Science and Society. *Bull. Amer. Meteor. Soc.* DOI: 10.1175/BAMS-D-15-00306.1

Skofronick-Jackson GM, Johnson BT, Munchak SJ. 2013. Detection Thresholds of Falling Snow from Satellite-Borne Active and Passive Sensors. *IEEE Transactions on Geoscience and Remote Sensing*. 51 : 4177 – 4189. DOI: 10.1109/TGRS.2012.2227763

Stanley T, Kirschbaum DB. 2017. A heuristic approach to global landslide susceptibility mapping. *Nat. Hazards*. 87: 145 – 164. DOI: 10.1007/s11069-017-2757-y

Stephens GL, Vane DG, Boain RJ, Mace GG, Sassen K, Wang Z, Illingworth AJ, O'Connor EJ, Rossow WB, Durden SL, Miller SD, Austin RT, Benedetti A, Mitrescu C, and CloudSat Science Team. 2002. The CloudSat mission and the A-Train: A new dimension of space-based observations of clouds and precipitation. *Bull. Amer. Meteorol. Soc.* 83 : 1771 – 1790. DOI: 10.1175/BAMS-83-12-1771

Tan BZ, Petersen WA, Tokay A. 2016a. A Novel Approach to Identify Sources of Errors in IMERG for GPM Ground Validation. *J. Hydrometeor.* 17 : 121 – 137. DOI: 10.1175/JHM-D-16-0079.1

Tan BZ, Petersen WA, Kirstetter P, Tian Y. 2016b. Performance of IMERG as a Function of Spatiotemporal Scale. *J. Hydrometeor.* 18 : 307 – 319. DOI: 10.1175/JHM-D-16-0174.1

Tang G, Wen Y, Gao J, Long D, Ma Y, Wan W, Hong Y. 2017. Similarities and differences between three coexisting spaceborne radars in global rainfall and snowfall estimation. *Water Resour. Res*., 53 : 3835 – 3853. DOI: 10.1002/2016WR019961

Tao J. Wu D, Gourley J, Zhang SQ, Crow W, Peters-Lidard CD, Barros A 2016. Operational hydrological forecasting during the IPHEx-IOP campaign – Meet the challenge. *J. Hydrol.* 531 : 434 – 456. DOI: 10.1016/j.jhydrol.2016.02.019

Tao WK, Wu D, Matsui T, Peters-Lidard C, Lang S, Hou A, Reinecker M, Petersen WA. 2013. The diurnal variation of precipitation during MC3E: A modelling study. *J. Geophys. Res*. 118 : 7199 – 7218. DOI: 10.1002/jgrd.50410/asset/jgrd50410

Tapiador, F.J., A. Navarro, V. Levizzani, E. García-Ortega, G.J. Huffman, C. Kidd, P.A. Kucera, C.D. Kummerow, H. Masunaga, W.A. Petersen, R. Roca, J.-L. Sánchez, W.-K. Tao, F. J. Turk, 2017: Global Precipitation Measurements for Validating Climate Models. *Atmos. Res*., **197**, 1-20. *doi:10.1016/j.atmosres.2017.06.021*

Thurai M, Gatlin PN, Bringi VN, Petersen W, Kennedy P, Notaros B, Carey LD. 2017. Toward Completing the Raindrop Size Spectrum: Case Studies Involving 2D-Video Disdrometer, Droplet Spectrometer, and Polarimetric Radar Measurements. *J. Appl. Meteor. Soc*. 56 : 877 – 896. DOI: 10.1175/JAMC-D-16-0304.1

Tian Y, Peters-Lidard C, Harrison K, Prigent C, Norouzi H, Aires F, Boukabara SA, Furuzawa F, Masunaga H. 2013. Quantifying Uncertainties in Land-Surface Microwave Emissivity Retrievals. IEEE Transactions on Geoscience and Remote Sensing. 52 : 829-840. DOI:10.1109/TGRS.2013.2244214

Tiira J, Moisseev DN, von Lerber A, D. Ori, Tokay A, Bliven LF, Petersen W. 2016. Ensemble mean density and its connection to other microphysical properties of falling snow as observed in southern Finland. *Atmos. Meas. Tech*. 9 : 4825 – 4841. DOI: 10.5194/amt-9-4825-2016

Tokay A, D'Adderio L, Porcu F, Wolff D, Petersen W. 2017. A Field Study of Footprint-Scale Variability of Raindrop Size Distribution. *J. Hydrometeor*. 16 : 1855 – 1868. DOI: 10.1175/JHM-D-15-0159.1

Toyoshima K, Masunaga H, Furuzawa FA. 2015. Early Evaluation of Ku- and Ka-Band Sensitivities for the Global Precipitation Measurement (GPM) Dual-Frequency Precipitation Radar (DPR). *SOLA*. 11: 14 – 17. DOI: 10.2141/sola.2015-004

Trenberth K. 2011. Changes in precipitation with climate change. *Clim. Res*. 47 : 123 – 138. DOI: 10.3354/cr00953

Turk FJ, Li L, Haddad ZS. 2014. A Physically Based Soil Moisture and Microwave Emissivity Data Set for Global Precipitation Measurement (GPM) Applications. *IEEE Transactions on Geoscience Remote Sensing*. 52 : 7637 – 7650. DOI: 10.1109/TGRS.2014.2315809

Tyynelä J, Chandrasekar V. 2014. Characterizing falling snow using multifrequency dual-polarization measurements. *J. Geophys. Res. Atmos*. 119 : 2169 – 8996. DOI: 10.1002/2013JD021369

Valle D, Zaitchik B, Feingold B, Spangler K, Pan W. 2013. Abundance of water bodies is critical to guide mosquito larval control interventions and predict risk of mosquito-borne diseases. *Parasit. Vectors*. 6 : 1 – 2. DOI: 10.1186/1756-3305-6-179

Vega M, Chandrasekar V, Carswell J, Beauchamp RM, Schwaller MR, Nguyen CM. 2014. Salient features of the dual-frequency, dual-polarized, Doppler radar for remote sensing of precipitation. *Radio Sci.* 49 : 1087 – 1105. DOI: 10.1002/2014RS005529

Vijayaraj V, Bright EA, Bhaduri BL. 2007. High Resolution Urban Feature Extraction for Global Population Mapping using High Performance Computing. *Proceedings of 2007 IEEE International geosciences and remote sensing symposium, IGARSS 2007.*

1253 von Lerber A, Moisseev D, Marks D, Petersen W, Harri A, Chandrasekar V. 2017. Validation of
1254 satellite-based snowfall products by using a combination of weather radar and surface
1255 observations. *J. Appl. Meteorol. and Clim.*, accepted with minor revision. .
1256
1257 Wang J, Adler R, Huffman G, Bolvin D. 2014. An Updated TRMM Composite Climatology of
1258 Tropical Rainfall and Its Validation. *J. Climate.* 27 : 273 – 284. DOI: 10.1175/JCLI-D-13-
1259 00331.1
1260
1261 Wen Y, Kirstetter P, Hong Y, Gourley JJ, Cao Q, Zhang J, Flamig Z, Xue X. 2016. Evaluation of
1262 a Method to Enhance Real-Time, Ground Radar–Based Rainfall Estimates Using Climatological
1263 Profiles of Reflectivity from Space. *J. Hydrometeor.* 17 : 761 – 775. DOI: 10.1175/JHM-D-15-
1264 0062.1
1265
1266 Wentz FJ, Draper D. 2016. On-Orbit Absolute Calibration of the Global Precipitation
1267 Measurement Microwave Imager. *J. Atmos. Oceanic Technol.* 33 : 1393 – 1412. DOI:
1268 10.1175/JTECH-D-15-0212.1
1269
1270 Wilheit T, Berg W, Ebrahami H, Kroodsma R, McKague D, Payne V, Wang J. 2015.
1271 Intercalibrating the GPM constellation using the GPM microwave imager (GMI). *Geoscience*
1272 *and Remote Sensing Symposium (IGARSS), 2015 IEEE International*. DOI:
1273 10.1109/IGARSS.2015.7326996
1274
1275 Williams CR, Bringi VN, Carey LD, Chandrasekar V, Gatlin PN, Haddad ZS, Meneghini R,
1276 Munchak SJ, Nesbitt SW, Petersen WA, Tanelli S, Tokay A, Wilson A, Wolff DB. 2014.
1277 Describing the shape of raindrop size distributions using uncorrelated raindrop mass spectrum
1278 parameters. *J. Appl. Meteor. Climatol*. 53 : 1282 – 1296. DOI: 10.1175/JAMC-D-13-076.1
1279
1280 Wolff DB, Marks D, Petersen WA. 2014. General application of the Relative Calibration
1281 Adjustment (RCA) technique for monitoring and correcting radar reflectivity calibration. *J.*
1282 *Atmos. Oceanic Technol*. 32 : 496 – 506. DOI: 10.1175/JTECH-D-13-00185.1
1283
1284 Wright DB, Kirschbaum DB, Yatheendradas S. 2017. Satellite Precipitation Characterization,
1285 Error Modelling, and Error Correction Using Censored Shifted Gamma Distributions. J.
1286 Hydrometeorol. DOI:10.1175/JHM-D-17-0060.1
1287
1288 Wu H, Adler RF, Tian Y, Huffman GJ, Li H, Wang J. 2014. Real-time global flood estimation
1289 using satellite-based precipitation and a coupled land surface and routing model. *Water Resour.*
1290 *Res.* 50 : 2693 – 2717. DOI: 10.1002/2013WR014710
1291
1292 You Y, Wang NY, Ferraro R, Rudlosky S. 2016. Quantifying the Snowfall Detection
1293 Performance of the Global Precipitation Measurement (GPM) Microwave Imager Channels over
1294 Land. *J. Hydrometeor.* 17 : 1101 – 1117. DOI: 10.1175/JHM-D-16-0190.1
1295 Zagrodnick, J. P., McMurdie, L. A., and Houze Jr., R. A., 2017: Stratiform Precipitation
1296 Processes in Cyclones Passing over a Coastal Mountain Range. *J. Atmos. Sci*., submitted.
1297
1298 Zaitchik BF, Feingold B, Valle D, Pan W. 2014. Integrating Earth Observations to Support

Malaria Risk Monitoring in the Amazon. *Earthzine*. [Available online at http://www.earthzine.org/2014/04/14/integrating-earth-observations-to-support-malaria-risk-monitoring-in-the-amazon/]

Zhang J, Howard K, Langston C, Kaney B, Qi Y, Tang L, Grams H, wang Y, Cocks S, Martinaitis S, Arthur A, Cooper K, Brogden J. 2016. Multi-Radar Multi-Sensor (MRMS) Quantitative Precipitation Estimation: Initial Operating Capabilities. *Bull. Amer. Meteor. Soc.* 97 : 621 – 638. DOI: 10.1175/BAMS-D-14-00174.1

Zhang SQ, Matsui T, Cheung S, Zupanski M, Peters-Lidard C. 2017. Impact of assimilated precipitation-sensitive radiances on the NU-WRF simulation of West African monsoon. *Mon. Wea. Rev.* DOI: 10.1175/MWR-D-16-0389.1

Tables

Table I. GPM constellation members, including the satellite, sensor, scanning mode, type of instrument, launch date and mission end. These include the passive microwave imagers (MWI), TRMM Microwave Imager (TMI), Special Sensor Microwave Image Sounder (SSMIS), GPM Microwave Imager (GMI), Advanced Microwave Scanning Radiometer-2 (AMSR2); the passive microwave sounders (MWS), Microwave Humidity Sounder (MHS), Advanced Technology Microwave Sounder (ATMS); and the radar or active microwave (AMW), Precipitation Radar (PR) and Dual-frequency Precipitation Radar (DPR). The spacecraft include NASA-JAXA GPM and TRMM satellites, the U.S. NOAA series, the U.S. Defense Meteorological Satellite Program (DMSP) series, the European Union Meteorological Satellites: MetOp-A and Metop-B, the French-Indian Megha-Tropiques satellite, the U.S. NPOESS Preparatory Project (NPP) satellite, and the Japanese Global Change Observation Mission 1st - Water (GCOM-W1) satellite. References are provided in Hou *et al*. (2014).

Satellite	Sensor	Scanning	Type	Launch	Until
TRMM	TMI	Conical	MWI	1997-11-27	2015-04-08
	PR	Cross-track	AMW		
DMSP F16	SSMIS	Conical	MWI	2003-10-18	
NOAA18	MHS	Cross-track	MWS	2005-05-20	
MetOpA	MHS	Cross-track	MWS	2006-10-19	
DMSP F17	SSMIS	Cross-track	MWI	2006-11-05	
NOAA19	MHS	Cross-track	MWS	2009-02-06	
DMSP F18	SSMIS	Conical	MWS	2009-10-18	
Megha-Tropiques	SAPHIR	Cross-track	MWS	2011-10-12	

NPP	ATMS	Cross-track	MWS	2011-10-28	
GCOM-W1	AMSR2	Conical	MWI	2012-05-17	
MetOpB	MHS	Cross-track	MWS	2012-09-17	
GPM-CO	GMI	Conical	MWI	2014-02-27	
	DPR	Cross-track	AMW		
DMSP F19	SSMIS	Conical	MWI	2014-04-03	2016-02-11

Table II. Summary description of GPM data products by the Product Level (1-4). Version 05 of the Level 2 algorithms became available for download in May 2017. National products are those designed and implemented by NASA or JAXA independently. Standard products require joint approval from a governing board composed of both NASA and JAXA representatives.

Product Level	Description	Coverage
Level 1B GMI	Geolocated and inter-calibrated brightness temperatures; Standard product	Swath, Instantaneous Field of View (IFOV)
Level 1B DPR	Geolocated and calibrated radar powers; JAXA National product	Swath, IFOV
Level 1C, GMI and partner radiometers, Note GMI 1B=GMI 1C	Inter-calibrated brightness temperatures; NASA National product	Swath, IFOV
Level 2 GMI (GPROF algorithm)	Radar enhanced precipitation retrievals; Standard product	Swath, IFOV
Level 2 partner radiometers (GPROF algorithm)	Radar enhanced precipitation retrievals from 1C; NASA National Product	Swath, IFOV
Level 2 DPR (DPR algorithm)	Reflectivities, sigma zero, characterization, PSD, precipitation with vertical structure; Standard product	Swath, IFOV (Normal Scan (NS) for Ku, High Sensitivity (HS) for Ka, and Matched Scan (MS) for Ku+Ka)
Level 2 combined	Precipitation; Standard product	Swath, IFOV (initially at

GMI+DPR (CORRA algorithm)		DPR Ku swath and then at GMI swath)
Level 3 Latent Heating (GMI, DPR, CORRA)	Latent heating and associated related parameters; Standard product	0.25° x 0.25° monthly grid
Level 3 Instrument Accumulations	GMI, partner radiometers, CORRA and DPR; Standard product	0.25° x 0.25° monthly grid
Level 3 Merged Products	Merger of GMI, partner radiometer, and IR; IMERG: NASA National product GSMaP: JAXA National product	As fine as: IMERG: 0.1° x 0.1° 30-minute grid GSMaP: 0.1° x 0.1° 60-minute grid
Level 4 Products	Model-assimilated precipitation forecast and analysis: NASA National product	Model temporal and spatial scales (planned)

1333

1334

1335 **Table III.** GPM product latency requirements and average latency statistics for the first three
1336 years of operation. NRT, research, and climate products, use varying levels of ancillary data.

Product	End-to-End (to user) Latency Requirement (90% of the time)	Percentage of Time Met (avg. to 25 Jan 2017)	Average Latency Statistics (averaged over # months, # files)
GMI L1 Tb	NRT: 1 hour	99.9	17.4 minutes (5mo, 29,581 files)
GMI GPROF L2 Precipitation	NRT: 1 hour	98.8	23.2 min (8 mo., 59,442 files)
	Research product: No requirement	N/A	Approximately 24 hours
	Climate Product: No requirement	N/A	Approximately 3 months
DPR L2 Precipitation	No requirement	N/A	76.2 min (20 mo., 20,053 files)
	Research product: No	N/A	Approximately 24 hours

	requirement		
DPR+GMI CORRA L2 Precipitation	NRT: 3 hours	98.0	83.5 min (20 mo., 26,239 files)
	Research product: No requirement	N/A	Approximately 24 hours
L3 IMERG	No requirement	N/A	Early Run: approximately 4 hrs, goal 3 hrs
			Late Run: approximately 12 hrs
			Late Run: approximately 3 months

Table IV. Primary GPM Ground Validation field campaigns. Note that this table does not include several GPM international partner-led campaigns that hosted smaller complements of NASA GPM instrumentation in Brazil, Canada, France, Italy, and South Korea. In the Instruments column, field campaigns use airborne remote sensing (R) and *in situ* microphysical (M), as well as ground-based instrumentation.

Campaign	Instruments	Description	Data Access
LPVEX 2010	R, M, radar, gauge disdrometer, ADMIRARI* radiometer, rawinsonde	*Light Precipitation Validation Experiment*. High-latitude cold, light rain over ocean and continental land surfaces. Joint with CloudSat GV.	https://ghrc.nsstc.nasa.gov/home/field-campaigns/lpvex
MC3E 2011	R, M, radar, gauge disdrometer, ADMIRARI radiometer rawinsonde	*Mid-latitude Continental Convective Clouds Experiment*. Warm-season mid-latitude convective and stratiform precipitation. Joint with the Department of Energy-Atmospheric Radiation Measurement facility. (Jensen *et al*., 2016)	https://ghrc.nsstc.nasa.gov/home/field-campaigns/mc3e https://www.arm.gov/data
GCPEX	R, M, radar,	*GPM Cold Season Precipitation*	https://ghrc.nsstc.nasa.gov/ho

2012	gauge disdrometer, ADMIRARI radiometer, rawinsonde	*Experiment*. Mid-latitude snow in synoptic and lake-effect environments. Joint with Environment Canada. (Skofronick-Jackson *et al*., 2016)	me/field-campaigns/ https://ghrc.nsstc.nasa.gov/home/field-campaigns/gcpex
IFloodS 2013	Radar, gauge, disdrometer, soil moisture, streamflow	*Iowa Floods Studies*. Warm-season mid-latitude mesoscale precipitation events and integrated hydrologic validation. Joint with Iowa Flood Center.	https://ghrc.nsstc.nasa.gov/home/field-campaigns/ifloods
IPHEx 2014	R, M, radar, gauge, disdrometer, rawinsonde	*Integrated Precipitation and Hydrology Experiment*. Warm-season orographic precipitation and integrated hydrologic validation (Barros *et al*., 2014)	https://ghrc.nsstc.nasa.gov/home/field-campaigns/iphex http://iphex.pratt.duke.edu/
OLYMPEX 2015/16	R, M, radar, gauge, disdrometer, rawinsonde, dropsonde, snow camera	*Olympic Mountains Experiment*. Cold-season orographic and oceanic rainfall and snow; integrated hydrologic validation. Joint with NASA Radar Experiment (RADEX). (Houze *et al*., 2017)	https://ghrc.nsstc.nasa.gov/home/field-campaigns/olympex http://olympex.atmos.washington.edu/

* ADMIRARI = Advanced Microwave Radiometer Rain Identification

Table V. List of TRMM and GPM societal benefit areas, topics, and specific uses of the data.

Societal Benefit Area	**Topic**	**Application**
Extreme Events and Disasters	Flooding	Incorporation in hydrologic routing models for flood estimation
	Landslides	Nowcasting of potential landslide activity, rainfall intensity and duration characteristics for landslide occurrence
	Tropical Cyclones	Improved characterization of tropical cyclone track and intensity
	Wildfires	Management and situational awareness of rainfall accumulation in affected areas
	Disaster Response	Situational awareness of extreme precipitation in potentially affected areas

	Re-insurance and Insurance	Definition of extreme precipitation thresholds to determine payouts for Microinsurance or improve situational awareness for precipitation climatologies
Water Resources & Agriculture	Drought	Evaluation of precipitation anomalies leveraging extended temporal record
	Water Resource Management	Assessment of freshwater input to basins and reservoirs to better quantify water fluxes
	Agricultural Applications and Food Security	Integration of precipitation data within agricultural models to estimate growing season onset, crop productivity and other variables
Weather and Climate Modelling	Numerical Weather Prediction	Assimilation of Level 1 brightness temperatures within NWP modelling for initializing model runs
	Land Surface Modelling	Data assimilation into land surface models to estimate environmental variables
	Climate Variability and Change	Verification and validation of seasonal and climate modelling
Public Health & Ecology	Disease Tracking	Tracking precipitation anomalies with environmental conditions for disease vectors or water-borne diseases
	Ecological Forecasting	Monitor changes in precipitation that are associated with migration patterns
Technology and Policy	Satellite services and Data Distribution	Supporting data distribution, ground systems services

Figure captions

Figure 1: GPM Core Observatory observations of a snow and rain event off the Carolina coastlines on 17 December 2016. Falling snow is shown in blues to purples, rain is in greens to reds. The GMI has a swath width of 885 km, DPR Ku has a swath of 245 km, while DPR Ka currently has a swath of 125 km (not shown). GMI channels have resolutions of 6-26 km while the DPR resolutions are at 5 km horizontally, and 250 m or 500 m vertically, depending on operating mode (Hou *et al.*, 2014).

Figure 2: Timeline of pre- and post-launch field campaigns for the GPM Ground Validation

program: 2010 Light Precipitation Validation Experiment (LPVEX), 2011 Mid-latitude Continental Convective Clouds Experiment (MC3E), 2012 GPM Cold Season Precipitation Experiment (GCPEX), 2013 Iowa Floods Studies (IFLOODS), 2014 Integrated Precipitation and Hydrology Experiment (IPHEx), 2015-2016 Olympic Mountains Experiment (OLYMPLEX).

Figure 3: The nearly global U.S. team's IMERG precipitation dataset provides rainfall rates every thirty minutes. This map of Version 04 Late Run data show rainfall accumulations from 16-22 July 2017.

Figure 4: Validation of DPR (a,b), CORRA (c,d) and GPROF GMI Products (e,f). The left column shows the satellite product verses ground validation reference for instantaneous rain rates at native resolution (5 km footprint for DPR and CORRA and 15 km EVOF for GPROF GMI. Dashed lines in left column indicate that each product meets the requirements of 0.2-110 mm h^{-1} for DPR and 0.2-60 for GMI. The right column shows results averaged over 50 km for bias and normalized mean absolute error (NMAE) random error to be < 25% at 10 mm h^{-1} and <50% at 1 mm h^{-1} as indicated in the green shaded area. The DPR data are from Version 05 and are the Matched Scan (Ku+Ka) retrievals

Figure 5: CloudSat falling snow estimates using several minimum detectable reflectivity thresholds as compared to DPR falling snow retrievals. Falling snow rate differences are in mm day^{-1} and averaged over 1°x1° latitude-longitude grid boxes for the period 03/2014-03/2016 for CloudSat and 03/2014-12/2016 for DPR. Differences are (CloudSat – GPM DPR Normal Scan [NS]) falling snow estimates for CloudSat reflectivities that are a) > -28 dBZ (all CloudSat data),

b) >5 dBZ, c) >8 dBZ, and d) >12 dBZ. Note that the official DPR falling snow products have been modified here to report the falling snow at the surface using the Sims and Liu (2015) temperature at 2m rain/snow indicator.

Figure 6: GPM-CO data from 2014-2017 showing the locations of precipitation features (PF) according to their size, DPR-Ku 20 dBZ, and 40 dBZ maximum echo top height.

Figure 7: Precipitation sampled during the GPM OLYMPEX overpass of 1523 UTC, 3 December 2015. a) NPOL 1.5° PPI of effective radar reflectivity factor (Z) with GPM track (bold line) and DPR Ku-band normal and matched scan boundaries indicated (light lines). A dashed line extending northeast of NPOL represents the orientation of cross-sections in panels (b)-(d); b) DPR Ku Normal Scan range-height cross-section of corrected-Z along the dotted line in (a), terrain shaded in black, position of NPOL indicated; c) NPOL range-height scan of Z along the DPR cross-section illustrating orographic enhancements over terrain and below the melting layer in regions of clutter-contaminated DPR data; d) as in (c) but NPOL radial velocity (negative values toward NPOL, positive values away).

Figure 8: Mean precipitation per person (PPP) (ton/year) at 0.1˚ resolution (Shepherd *et al.*, 2016), calculated using IMERG precipitation information and population density from LandScan global population dataset (Vijayaraj *et al.*, 2007).

Figure 9: Distribution of annually averaged landslide nowcasts using a model that brings together TMPA precipitation data and a global susceptibility map (Stanley and Kirschbaum,

2017).

Figure 10: GPM IMERG data enabled estimates of cholera risk following the passage of Hurricane Matthew across Haiti on 1-2 October 2016. Plots show a) Hurricane Matthew's track, highlighting the study area in Haiti, b) September 2016 IMERG precipitation anomalies, c) 14 September-13 October 2016 precipitation anomalies, d) Cholera risk map based on pre-hurricane hydro-climatic conditions, and e) Cholera risk map based on 2 weeks post hurricane hydroclimatic conditions. Figure modified from Khan *et al.* (2017).

1417

1418 Figure 1.

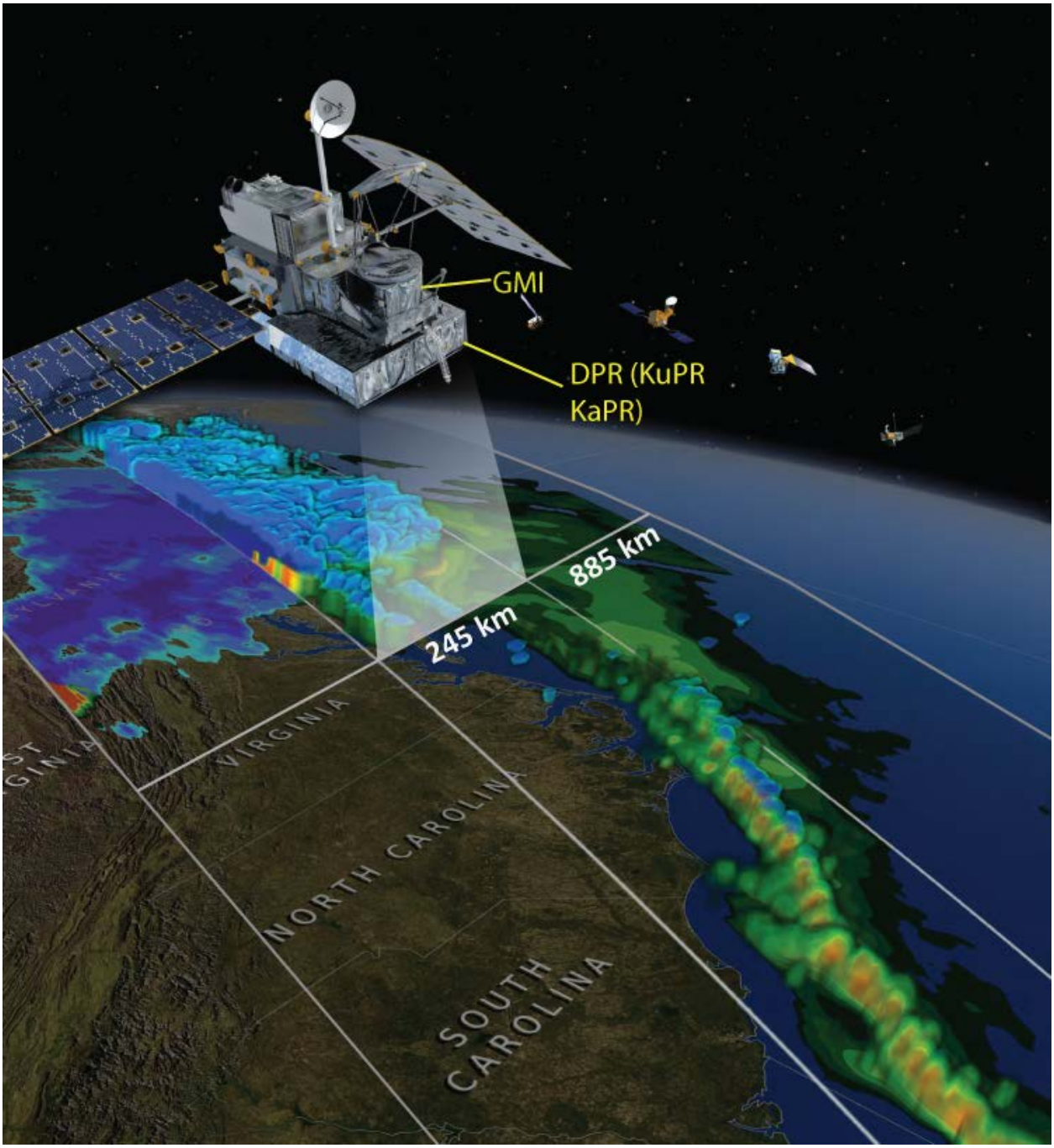

1419

1420

1421

1422

1423

Figure 2.

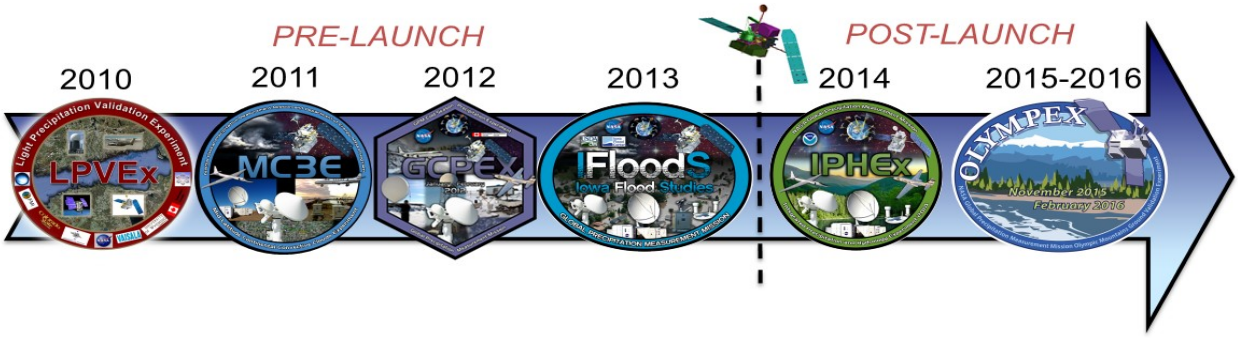

Figure 3.

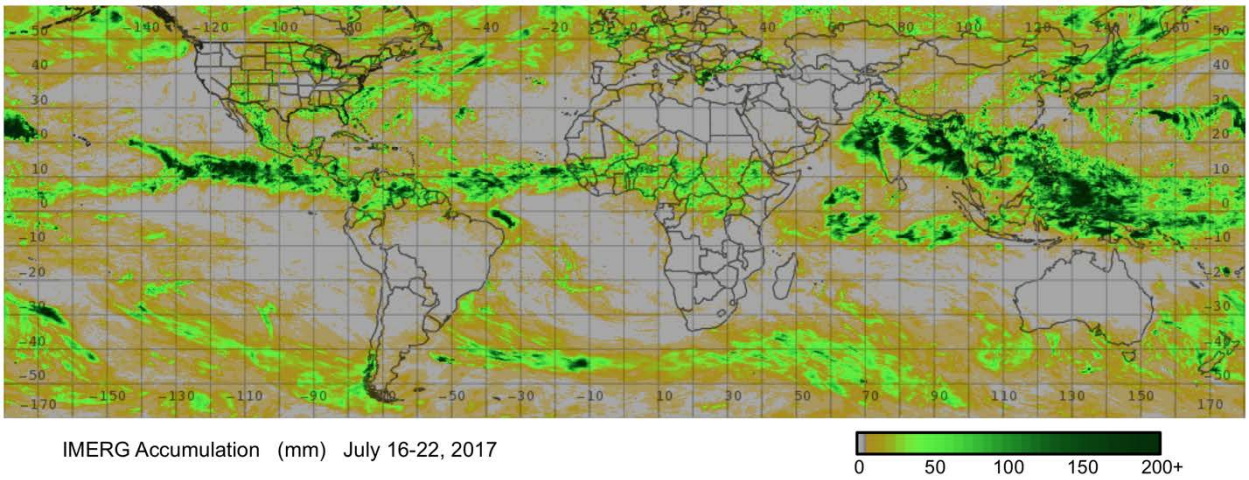

1440 Figure 4.

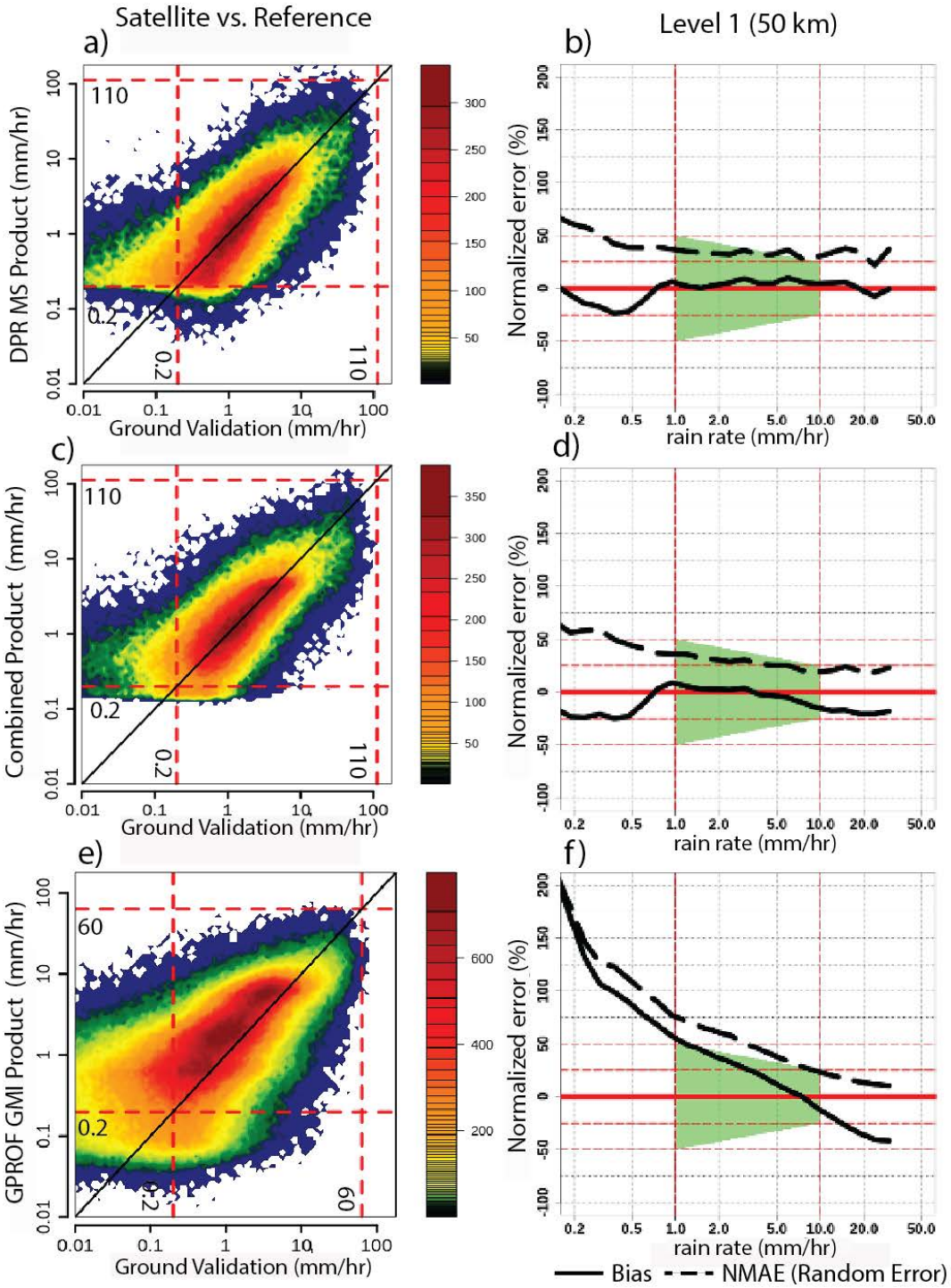

1441

1442

1443

1444

1445 Figure 5.

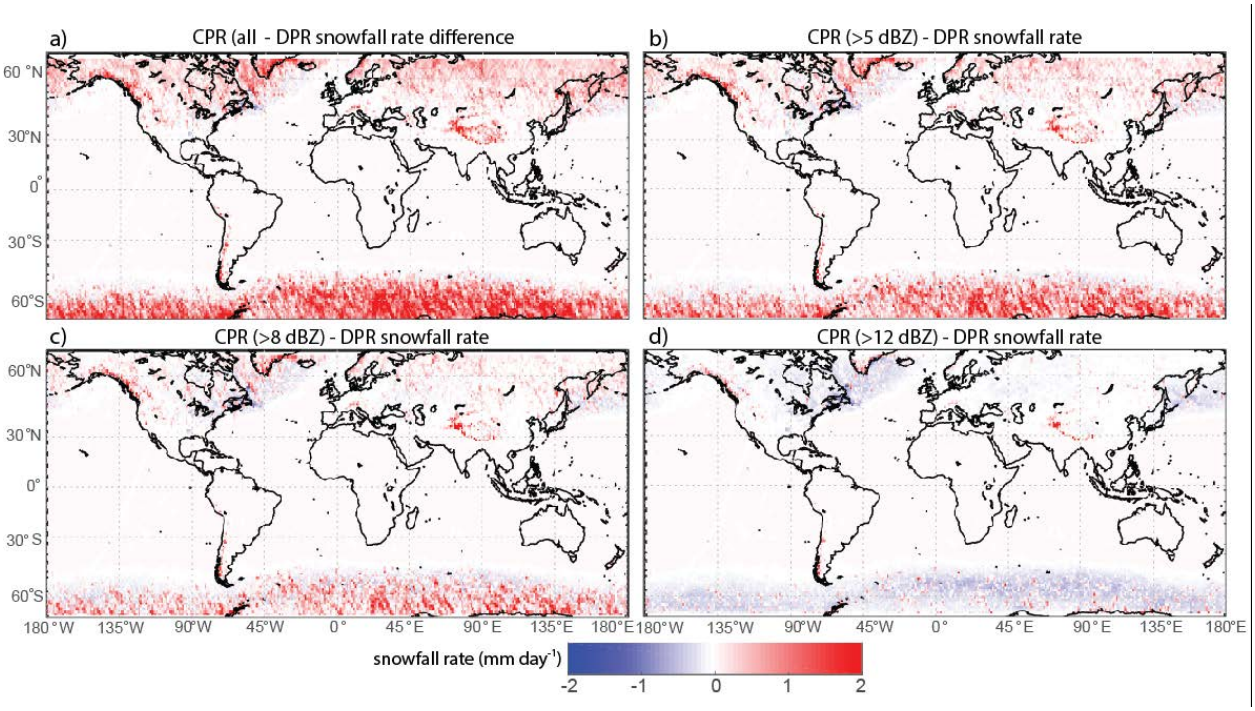

1446

1447

1448

1449

1450

1451

1452

1453

1454

1455

1456

1457

1458

1459

1460

1461

1462

1463 Figure 6.

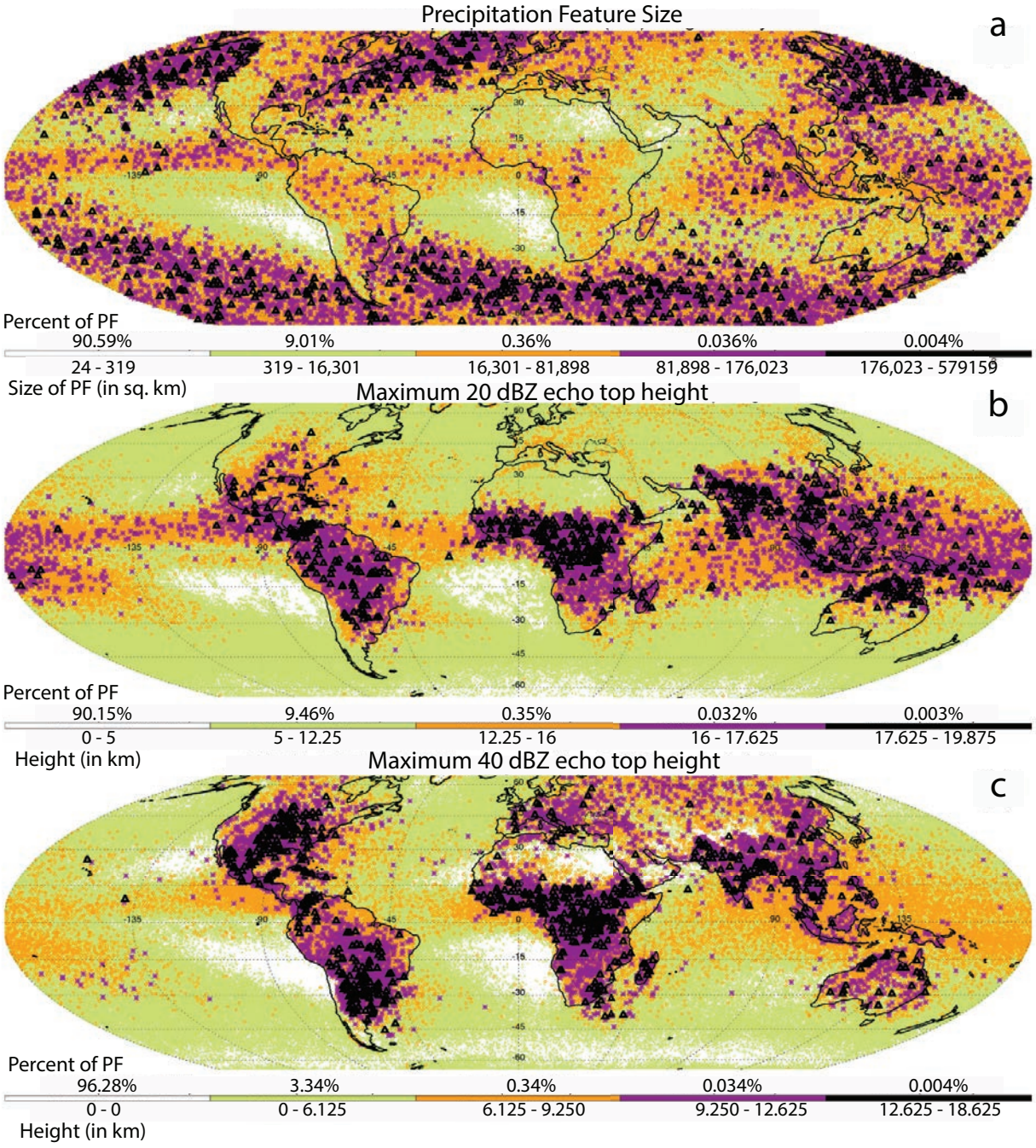

1464

1465

1466

1467

1468

1469

1470 Figure 7

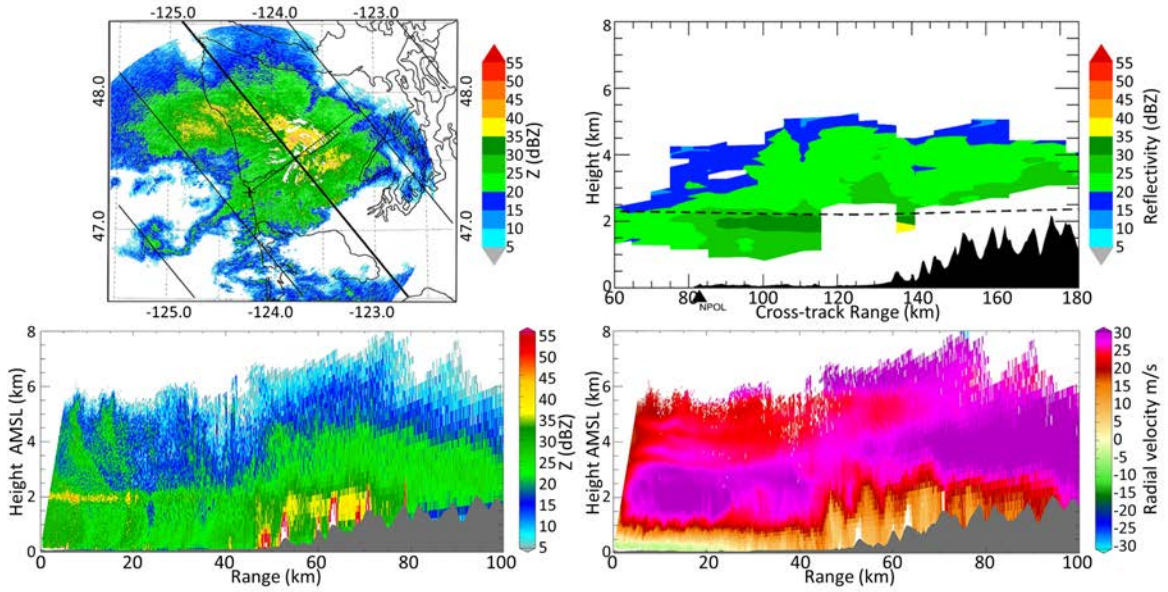

1471

1472 Figure 8

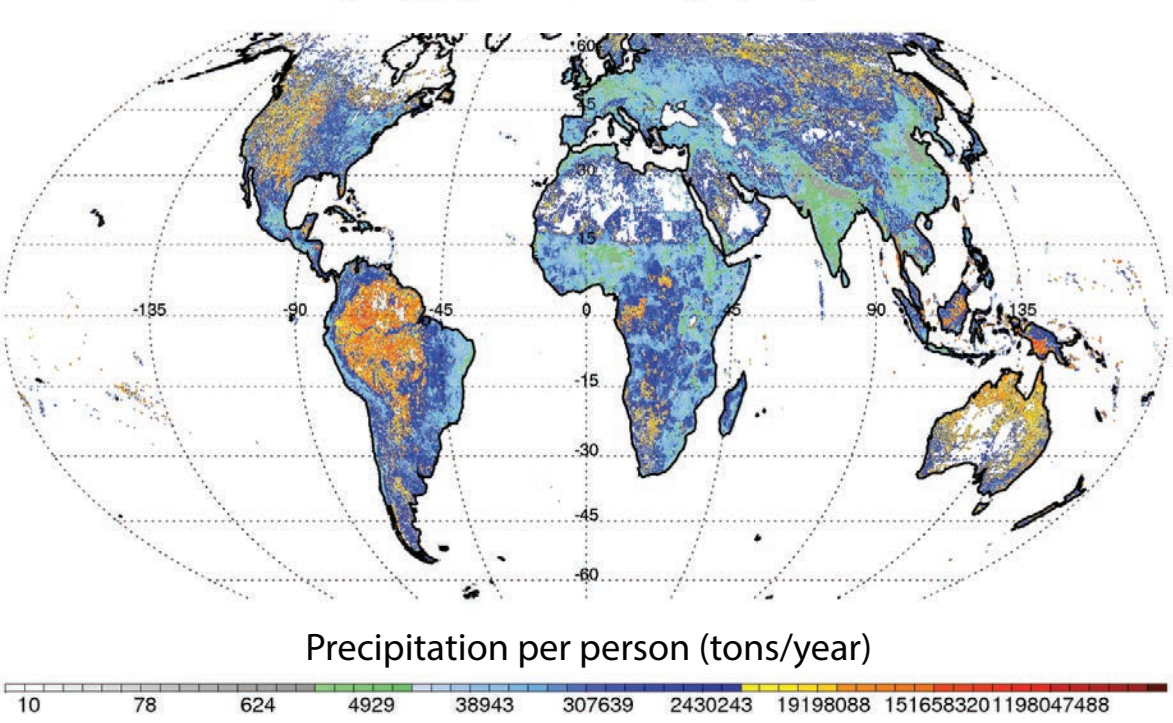

1473

1474

1475 Figure 9

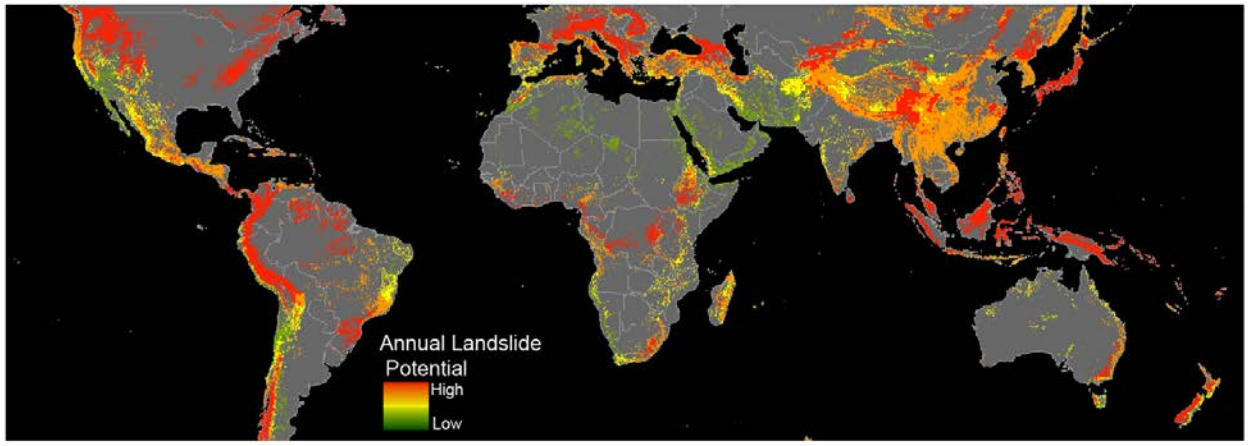

1476

1477

1478

1479 Figure 10

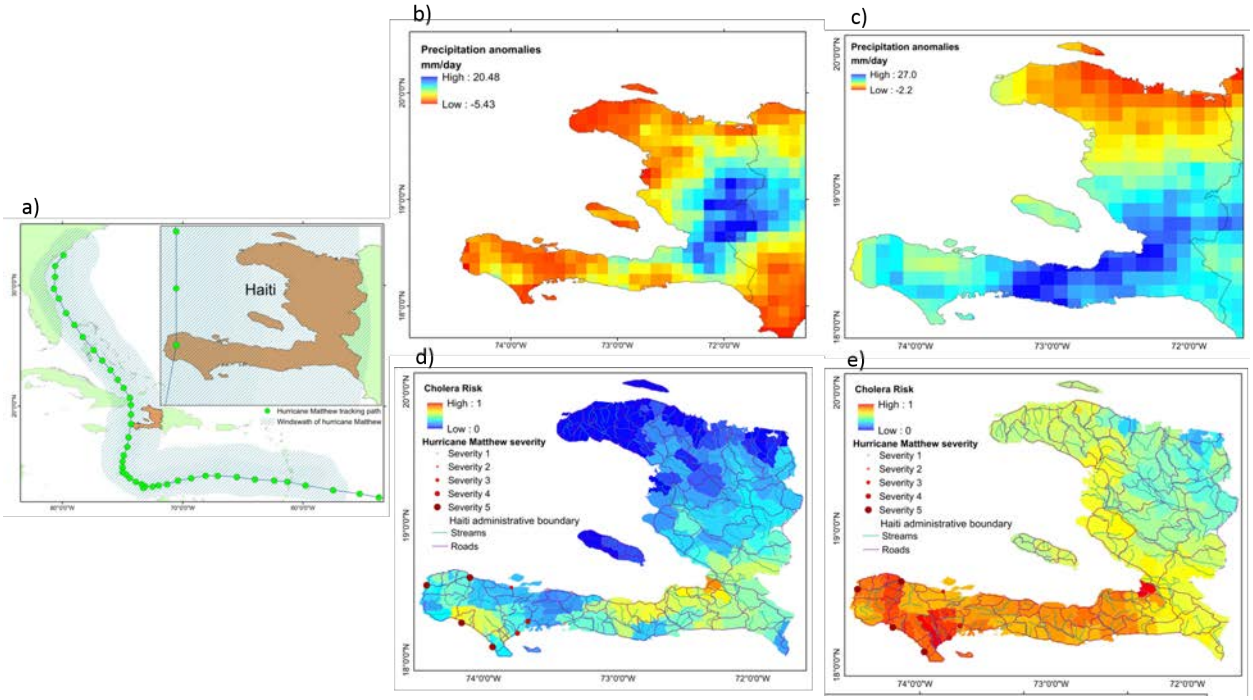

1480

1481

1482